ORIGINAL RESEARCH

ChGn-2 Plays a Cardioprotective Role in Heart Failure Caused by Acute Pressure Overload

Andreas Haryono (iD), MD, MSc; Koji Ikeda (iD), MD, PhD; Dhite Bayu Nugroho, MD, PhD; Takehiro Ogata, MD, PhD; Yumika Tsuji (iD), MD; Satoaki Matoba, MD, PhD; Kensuke Moriwaki, PhD; Hiroshi Kitagawa (iD), PhD; Michihiro Igarashi (iD), PhD; Ken-ichi Hirata, MD, PhD; Noriaki Emoto (iD), MD, PhD

BACKGROUND: Cardiac extracellular matrix is critically involved in cardiac homeostasis, and accumulation of chondroitin sulfate glycosaminoglycans (CS-GAGs) was previously shown to exacerbate heart failure by augmenting inflammation and fibrosis at the chronic phase. However, the mechanism by which CS-GAGs affect cardiac functions remains unclear, especially at the acute phase.

METHODS AND RESULTS: We explored a role of CS-GAG in heart failure using mice with target deletion of ChGn-2 (chondroitin sulfate N-acetylgalactosaminyltransferase-2) that elongates CS chains of glycosaminoglycans. Heart failure was induced by transverse aortic constriction in mice. The role of CS-GAG derived from cardiac fibroblasts in cardiomyocyte death was analyzed. Cardiac fibroblasts were subjected to cyclic mechanical stretch that mimics increased workload in the heart. Significant CS-GAGs accumulation was detected in the heart of wild-type mice after transverse aortic constriction, which was substantially reduced in ChGn-2$^{-/-}$ mice. Loss of ChGn-2 deteriorated the cardiac dysfunction caused by pressure overload, accompanied by augmented cardiac hypertrophy and increased cardiomyocyte apoptosis. Cyclic mechanical stretch increased ChGn-2 expression and enhanced glycosaminoglycan production in cardiac fibroblasts. Conditioned medium derived from the stretched cardiac fibroblasts showed cardioprotective effects, which was abolished by CS-GAGs degradation. We found that CS-GAGs elicits cardioprotective effects via dual pathway; direct pathway through interaction with CD44, and indirect pathway through binding to and activating insulin-like growth factor-1.

CONCLUSIONS: Our data revealed the cardioprotective effects of CS-GAGs; therefore, CS-GAGs may play biphasic role in the development of heart failure; cardioprotective role at acute phase despite its possible unfavorable role in the advanced phase.

Key Words: cardiac fibroblasts ■ cardiomyocytes ■ chondroitin sulfate glycosaminoglycan ■ extracellular matrix ■ heart failure ■ mechanical stretch

Cardiac extracellular matrix (ECM) provides structural support and modulates the activity of cytokines and growth factors in the heart.[1] Cardiac ECM, which is composed of collagens, glycoproteins, proteoglycans, and glycosaminoglycans, undergoes extensive remodeling during the progression of heart diseases.[2] These changes in ECM components are critically involved in pathological cardiac remodelings such as cardiac hypertrophy and fibrosis.[3]

Proteoglycans are composed of a protein core and glycosaminoglycan chains including chondroitin sulfate (CS), heparan sulfate, dermatan sulfate, and heparin.[4] Chondroitin sulfate (CS) is one of the major glycosaminoglycans and is composed of N-acetylgalactosamine

CLINICAL PERSPECTIVE

What Is New?

- Chondroitin sulfate glycosaminoglycans (CS-GAGs) protect cardiomyocyte from acute injury stress.
- Mechanical stretch enhances ChGn-2 (chondroitin sulfate N-acetylgalactosaminyltransferase) expression and promotes CS-GAGs production in cardiac fibroblasts.

What Are the Clinical Implications?

- CS-GAGs are an attractive therapeutic target against heart failure.
- ChGn-2 is a potential target for modulation of CS-GAGs production in the heart.
- CS-GAGs might have biphasic effects on cardiac function and remodeling in heart failure; stage-dependent approaches for CS-GAGs-targeted therapy are required to treat heart failure.

Nonstandard Abbreviations and Acronyms

ChGn-2	chondroitin sulfate N-acetylgalactosaminyltransferase-2
CM	conditioned medium
CS-GAG	chondroitin sulfate glycosaminoglycan
HCF	human cardiac fibroblast
MCF	mouse cardiac fibroblast
NRC	neonatal rat cardiomyocyte
TAC	transverse aortic constriction
WT	wild type

and glucuronic acid.[5] CS has been shown to play an important role in post-injury recovery of nervous system by modulating the immune system.[6–8] In cardiovascular system, CS accumulation has been shown in the failing heart, and detrimental roles of CS in heart failure by enhancing cardiac inflammation have been reported.[9] At the developmental stage, CS expression is required for cardiac atrioventricular canal development in zebra fish,[10] and it also play a role in cardiac differentiation of embryonic stem cells.[11] Also, several reports have shown a possible role of CS in the formation of atherosclerotic plaque.[12–14]

CS-glycosaminoglycans (CS-GAGs) chain is synthesized through cooperation between numerous enzymes.[15] ChGn-2 (chondroitin sulfate N-acetylgalactosaminyltransferase-2) is an enzyme that elongates CS chains in cooperation with chondroitin

4-sulfotransferase 1.[16] ChGn-2 is expressed ubiquitously in all tissues of human.[17] Deletion of ChGn-2 was previously shown to reduce and shorten the length of CS chain in mouse tissues.[18–20] This reduction of CS-GAGs chain showed beneficial effects in the prevention of atherosclerosis by reducing the oxidized LDL accumulation in the intima and on the macrophage surface.[18,19] On the other hand, another perspective was reported that CS administration attenuated atherosclerosis in ApoE-deficient mice potentially by inhibiting foam cell formation of macrophages.[21]

Recently, it has been reported that excess accumulation of CS-GAGs in the heart deteriorates heart failure by retaining inflammatory cytokines in the advanced stage[9]; however, whether and by which mechanism CS-GAGs are causally involved in heart failure remain unclear. In this study, we revealed another facet of CS in heart failure by exploring a role of CS in heart failure caused by acute pressure overload. Loss of ChGn-2, which causes reduction in CS-GAG chain, results in deteriorated cardiac hypertrophy, early cardiac dilatation, and increased cardiomyocyte apoptosis, leading to severe heart failure. We also revealed that CS-GAGs protect cardiomyocytes from death through dual pathway; direct interaction with CD44 and indirect activation of insulin-like growth factor-1.

METHODS

The data that support the findings of this study are available from the corresponding author upon reasonable request.

Materials

Materials and antibodies used are shown in Table S1.

Ethics Statement

All experimental animal procedures were approved by the Institutional Animal Care and Use Committee (2016-025, 2017-030, 2018-014) and carried out according to the Kobe University Animal Experimentation Regulation, Animal Facility of Kobe Pharmaceutical University, and the *Guide for the Care and Use of Laboratory Animals* published by the US National Institute of Health.

Animal Models

Mice lacking ChGn-2 (ChGn-2$^{-/-}$) on C57BL/6 genetic background were obtained from Niigata University.[22] ChGn-2 exon 5 that encodes a DXD motif, which is a binding site for Mn^{2+} that is essential for N-acetylgalactosamine transferase activity, was deleted. Mice were maintained under a 12-hours light-dark cycle and fed standard CRF-1 mouse chow (Charles River

Laboratories International, Inc., Wilmington, MA, USA) ad libitum. Both male and female mice were subjected to transverse aortic constriction (TAC) procedure. All animal experiments were approved by the animal experimentation committee of Kobe Pharmaceutical University.

TAC Technique

Acute pressure overload model was generated by TAC according to Rockman technique.[23] Briefly, mice were anesthesized using 1% to 5% isoflurane and immobilized in prone position. Fur in chest area was clipped and surgical field sterilized using 70% ethanol. Intubation was done, and then connected to ventilator. Partial thoracotomy to the second rib was performed under surgical microscope. Thymus and fat tissue was gently separated from aortic arch using fine tip forceps. Following identification of the transverse aorta, a small piece of a 6.0-silk suture is placed between the innominate and left carotid arteries. Transverse aorta was contricted with blunt 27-gauge needle as spacer. Rib cage and skin were then closed using 6.0-silk suture.

Echocardiography

Echocardiography was performed at days 0, 3, 7, and 14 to assess the left ventricular (LV) systolic functions. Echocardiography was performed according to previous reports.[24–27] Briefly, mice were anesthetized using 2% isoflurane. Anesthesia was controlled so that the heart rate was maintained at 400 to 500 beats/min. Mice were then placed to pad in prone position and chest hair was removed. Echo gel was placed on shaved chest and the 2-dimensional image of LV short axis and LV long axis were visualized using Acuson X-300 (Siemens).

LV internal dimensions, left ventricular posterior wall diameter, LV interventricular septal thicknesses at diastole and systole were measured from M-mode images at the level of the papillary muscles. Fractional shortening, ejection fraction, stroke volume, cardiac output and LV mass were calculated by using the following formulas[24,25]:

$$FS\ (\%) = 100 \times \left[(LVIDd - LVIDs)/LVIDd \right]$$

$$EF\ (\%) = 100 \times \left[(LVIDd)^3 - (LVIDs)^3 /LVIDd^3 \right]$$

$$SV = (LVIDd)^3 - (LVIDs)^3$$

$$CO = SV \times HR$$

$$LV\ mass = 1.05 \times \left[(IVSd + LVIDd + PWd)^3 - LVIDd^3 \right]$$

Tissue Collection From Mice

Mice were put into deep anesthesia by 5% isoflurane inhalation and euthanized by cervical dislocation 14 days after TAC or sham surgery. Immediately, the skin was incised from abdominal until chest area, peritoneal cavity was opened and inferior vena cava was dissected. Subsequently, mice rib cage was opened, and the exposed heart was perfused with PBS. The heart was then excised and weighted. Body weight was measured before sacrifice, and left tibia length was measured after euthanasia. Hearts were either snap-frozen in liquid nitrogen or fixed with 4% paraformardehyde for histological analysis.

Histological Analysis

Formalin fixed, parrafin-embedded heart sections were stained with Masson trichrome[28] and Alcian Blue[18] as described previously. Fibrosis area in the heart was quantified using Image J software.[29] For detection of cardiomyocyte apoptosis, heart sections were immunostained using anti-cardiac troponin T (Abcam, ab10214; 1:400 dilution), followed by incubation with alexa fluor 594-conjugated anti-mouse IgG antibody (Invitrogen, A-21203; 1:500 dilution). Subsequently, apoptotic cells were detected using the in situ Cell Death Detection Kit (Roche, #11684795910). For CS detection, heart sections were immunostained using antibody anti-CS A (2H6) antibody (Cosmo Bio, NU-07-001; 1:5000 dilution), followed by incubation with fluorescein-conjugated anti-mouse IgM antibody (TCI Chemicals, G0453; 1:200 dilution). For both immunostaining, mouse IgG blocking reagent and M.O.M antibody diluent from M.O.M immunodetection kit (Vector Laboratories, PK-2200) were used for reducing background signal.

RNA Isolation and Quantitative Polymerase Chain Reaction

RNAs were extracted from heart tissue or cells using RNA isoplus (Takara, #9109), and then purified using Nucleo Spin RNA Clean Up kit (Macherey-Nagel, 740948.50). cDNA was synthetized from 1 µg RNA using PrimeScript RT reagent Kit (Takara, RR047A). Quantitative real-time polymerase chain reaction was performed using LightCycler 96 Instrument (Roche Life Science) with SYBR Green real-time polymerase chain reaction master mix. Primers used were shown in Table S2.

Protein Extraction and Immunoblotting

Heart tissue and cells were homogenized in RIPA buffer containing protease (Sigma-aldrich, P8340) and phophatase inhibitors (1 mmol/L sodium orthovanadate and 5 mmol/L sodium fluoride). Protein concentration

was determined using DC protein assay kit (Bio-Rad, #5000116). Equal amounts of proteins (20–30 μg) were run on SDS-PAGE gel, and transferred onto nitrocellulose membrane as described previously.[30] The membrane was probed with first antibody, followed by incubation with secondary antibody diluted in Can Get Signal Immunoreaction Enhancer Solution (Toyobo, #NKB-101). Subsequently, the membrane was incubated with Clarity Western ECL Substrate (Bio-Rad, #1705061), and signals were detected using ChemiDoc XRS Plus (Bio-Rad).

Chondroitin-4-sulfate Dot BLOT

Nitrocellulose membrane was prewetted with PBS and air dried 30 minutes at room temperature; 2 μL of isolated protein were directly blotted to nitrocellulose membrane. Membranes were then air dried for 30 minutes at room temperature, and blocked with 5% BSA in TBS-T. Subsequently, membranes were incubated with anti-chondroitin sulfate A (2H6) (Cosmo Bio, #NU-07-001) at 1:5000 dilution, followed by incubation with HRP-labeled secondary antibody (TCI Chemicals, #G0417) at 1:2000 dilution. Signals were elicited by Clarity Western ECL Substrate (Bio-Rad, #1705061), and detected using ChemiDoc XRS Plus (Bio-Rad).

Cell Culture

Human primary cardiac fibroblasts (HCFs, #C12375) was purchased from PromoCell, and cultured in Fibroblast Growth Medium (PromoCell, #C-23110). HCFs with passage number 6 were used for all experiments. Mouse cardiac fibroblasts (MCFs) were isolated and cultured according to previous publication.[31] MCFs with passage number 3 were used for all experiments. Neonatal rat cardiomyocytes (NRCs) were isolated, and cultured as described previously.[32] H9C2 cells was purchased from ATCC, cultured in DMEM high glucose supplemented with 10% FBS (Gibco, #10270106) and 1% ABAM (Gibco, #15240062).

Cell Stretching Experiment and Fibroblast Conditioned Medium Preparation

HCFs and MCFs were cultured on silicone elastic membranes when subjected to the mechanical stretch stimuli. At confluence, growth medium was changed into serum free fibroblast basal medium. Then, cells were subjected to cyclic stretch of 10% elongation at 60 cycles/min for 24 hours, which has been reported to resemble cardiac overload in vivo.[33–35] The cyclic mechanical stretch was generated by the STREX Cell Stretching Systems (Strex, #STB-1400). After 24 hours of stretch stimuli, the conditioned medium (CM) was collected and centrifuged at 300g to remove suspended cells. Resulting supernatant was filtered using 0.2 μm DISMIC-13CP syringe filter (Advantec, #13CP020AS). To prepare CM from the cells without stretch stimuli, cells were cultured on silicone elastic membranes, and incubated for 24 hours in the absence of stretch stimuli.

Apoptosis Assay

Cardiac cell apoptosis was induced by using doxorubicin. Briefly, cells were grown until confluent in 6 or 96 well plates, and then incubated in serum free medium or serum free CM for 18 hours, followed by treatment with doxorubicin for further 5 hours. Doxorubicin was used at 1 μmol/L, unless otherwise stated. Apoptosis was assessed by immunoblotting for cleaved caspase-3 and TUNEL staining using in situ Cell Death Detection Kit (Roche, #11684795910).
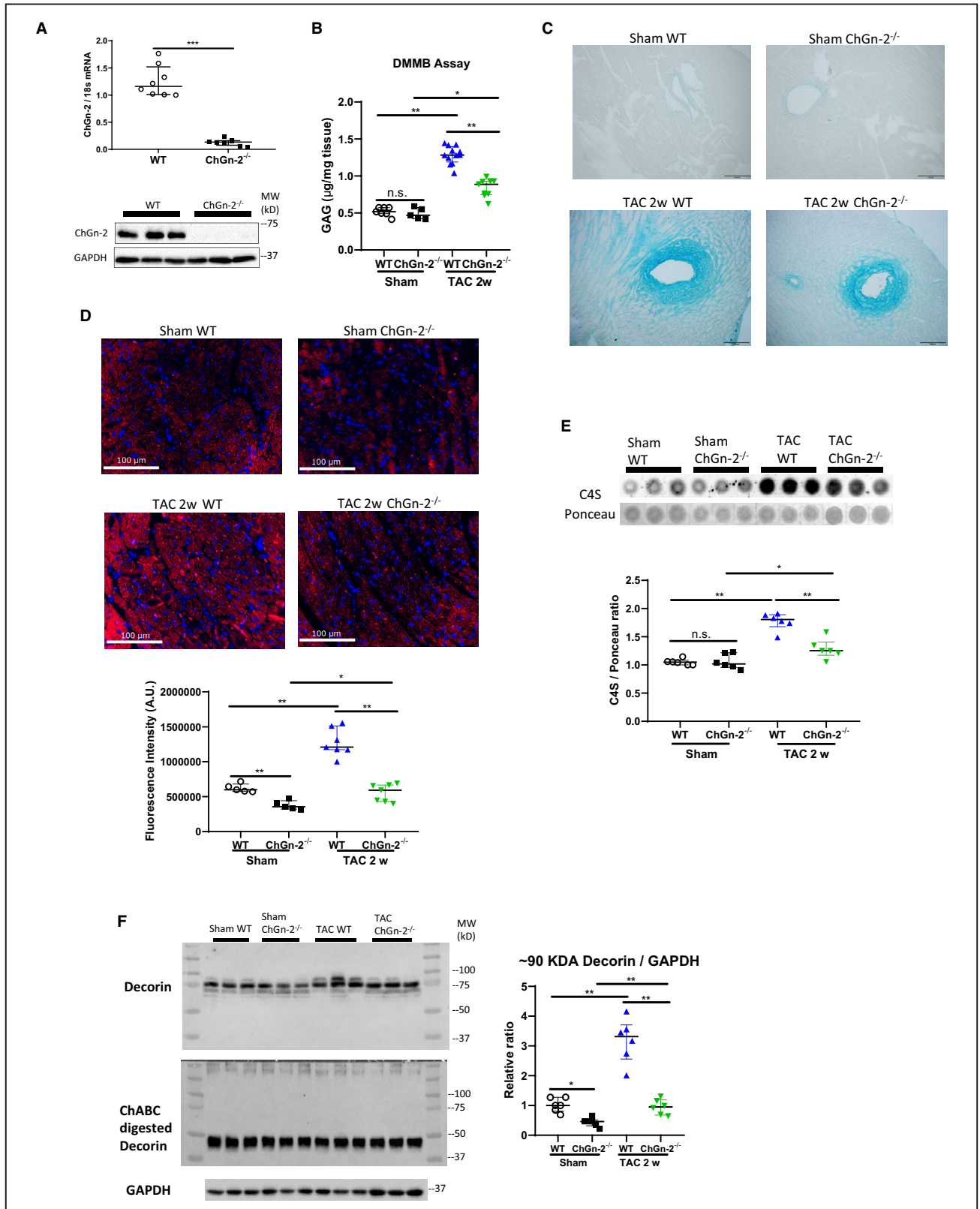
Retrovirus Preparation

To construct a retrovirus expression vector for ChGn-2 proteins, pcDNA3.1/Myc-His-hChGn-2 plasmid[19] were digested with BamHI and AflII. The

Figure 1. Accumulation of chondroitin sulfate glycosaminoglycans in the heart after acute pressure overload is reduced in ChGn-2$^{-/-}$ (chondroitin sulfate N-acetylgalactosaminyltransferase-2) mice.

A, Quantitative real time polymerase chain reaction (n=8 for each group) and immunoblotting (n=3 for each group) analysis for ChGn-2 in the heart of wild-type (WT) and ChGn-2$^{-/-}$ mice. Molecular weight (MW) for protein ladders are shown. **B**, Quantification of extracted total glycosaminoglycans using 1,9-dimethylmethylene blue assay in the heart of WT and ChGn-2$^{-/-}$ mice in either sham or transverse aortic constriction (TAC) condition (n=7 for sham WT, n=5 for sham ChGn-2$^{-/-}$, n=12 for TAC WT, n=9 for TAC ChGn-2$^{-/-}$). **C**, Representative images for Alcian blue staining in the heart of WT and ChGn-2$^{-/-}$ mice in either sham or TAC condition; bars: 100 μm. **D**, Representative images of immmunofluorescence for chondroitin-4-sulfate (C4S) in the heart of WT and ChGn-2$^{-/-}$ in either sham or TAC condition. C4S fluorescence intensity was quantified (n=5 for sham WT, n=5 for sham ChGn-2$^{-/-}$, n=7 for TAC WT, n=7 for TAC ChGn-2$^{-/-}$); bars: 100 μm. C4S, red; and 4',6-diamidino-2-28 phenylindole dihydrochloride, blue. **E**, Dot blot analysis for C4S in the heart of WT and ChGn-2$^{-/-}$ mice in either sham or TAC conditions. C4S expression was quantified and normalized to total protein assessed by the ponceau staining (n=6 for each group). **F**, Immunoblotting for decorin in heart of WT and ChGn-2$^{-/-}$ mice in either sham or TAC conditions. High molecular weight decorin protein expression was quantified and normalized to GAPDH expression (n=6 for each group). Bottom blot shows the results after degradation of glycosaminoglycans by chondroitinase ABC treatment. Molecular weight (MW) for protein ladders are shown. Data represent median and interquartile range. *P<0.05, **P<0.01, and ***P<0.001. Statistical analyses were performed using Wilcoxon rank-sum test **(A)** or Kruskal–Wallis test followed by Wilcoxon rank-sum test **(B, D, E, and F)**. 18s indicates 18s ribosomal RNA; A.U., arbitrary unit; C4S, chondroitin-4-sulfate; ChABC, chondroitinase ABC; ChGn-2, chondroitin sulfate N-acetylgalactosaminyltransferase-2; DMMB, 1,9-dimethylmethylene blue; TAC, transverse aortic constriction; and WT, wild-type.

1.7-kb *Bam*HI-*Afl*II fragments were blunted using T4 polymerase, and then inserted into *Hpa*I site of pMCSV-neo vector. Resulting pMSCV-neo-hChGn-2 plasmid was co-transfected with pVSV-G viral envelop plasmid into GP2-293 cells to prepare retrovirus carrying hChGn-2. Control viruses carrying GFP

were prepared using pMSCV-neo-GFP plasmid. Retroviruses in the medium were aliquoted and kept at −80 °C until use.

Glycosaminoglycans Analysis With Dimethylmethylene Blue Assay

Glycosaminoglycans from the heart tissue or conditioned mediums were isolated and quantified by 1,9-dimethylmethylene blue assay according to previous publications.[36,37]

Statistical Analysis

A series of statistical analyses were performed using GraphPad Prism software version 8 (GraphPad Software, Inc) and Stata 17 (Stata Corp LLC). Because of the small sample size and the possibility that assumptions of normality and equal variance were not met for some of the data sets, we applied hypothetical tests using non-parametric methods. Differences between 2 groups were analyzed using Wilcoxon rank-sum test. Differences among groups >3 were analyzed using Kruskal−Wallis test. As a post hoc test, Wilcoxon rank-sum test was performed for pairwise comparison. Numerical data were summarized as median and interquartile range. Survival data were summarized using the Kaplan−Meier method and differences between groups were analyzed using

log-rank test. $P<0.05$ was considered statistically significant.

RESULTS

## Loss of ChGn-2 Exacerbates the Cardiac Dysfunction Caused by Acute Pressure Overload

Acute pressure overload was induced by TAC using wild-type (WT) and ChGn-2$^{-/-}$ mice (Figure 1A). After 2 weeks of TAC, significant glycosaminoglycans accumulation was detected in the heart, assessed by dimethylmethylene blue assay, Alcian blue staining, immunofluorescence staining for chondroitin-4-sulfate, and immunoblotting for chondroitin-4-sulfate (Figure 1B through 1E). Loss of ChGn-2 significantly reduced the glycosaminoglycan accumulation after 2 weeks of TAC (Figure 1B through 1E). Reduced glycosaminoglycan contents in the heart of ChGn-2$^{-/-}$ mice were further supported by the immunoblotting for decorin that is highly glycosylated by CS-GAGs. High molecular weight decorin that has long CS-GAG chains was increased in the heart of WT mice after TAC, while less increase was detected in the heart of ChGn-2$^{-/-}$ mice (Figure 1F). These data indicate that acute pressure overload causes enhanced glycosaminoglycans accumulation in the heart, and loss of ChGn-2 ameliorates it.

Figure 2. ChGn-2$^{-/-}$ (chondroitin sulfate N-acetylgalactosaminyltransferase-2) mice exhibit severe left ventricle dysfunction after acute pressure overload.

A, Representative echocardiographic images in wild-type (WT) and ChGn-2$^{-/-}$ mice in either sham or transverse aortic contriction (TAC) group 2 weeks after surgery. White bars: 200 msec; red bars: 2 mm. **B**, Left ventricular systolic function was analyzed by the fractional shortening at day 0, 3, 7, 10, and 14 days after TAC (n=6 for sham WT, n=5 for sham ChGn-2$^{-/-}$, n=8 for TAC WT, n=8 for TAC ChGn-2$^{-/-}$). Kruskal−Wallis test followed by Wilcoxon rank-sum test was used to analyze the difference of fractional shortening between the groups at each time point. $^{\$\$}P<0.01$ between sham WT and TAC WT. $^{++}P<0.01$ between sham ChGn-2$^{-/-}$ and TAC ChGn-2$^{-/-}$. $^{\%\%}P<0.01$ and $^{\%\%\%}P<0.001$ between TAC WT and TAC ChGn-2$^{-/-}$. **C**, Left ventricular systolic function was analyzed by the ejection fraction at day 0, 3, 7, 10, and 14 days after TAC (n=6 for sham WT, n=5 for sham ChGn-2$^{-/-}$, n=8 for TAC WT, n=8 for TAC ChGn-2$^{-/-}$). Kruskal−Wallis test followed by Wilcoxon rank-sum test was used to analyze the difference of ejection fraction between the groups. $^{\$\$}P<0.01$ between sham WT and TAC WT. $^{++}P<0.01$ between sham ChGn-2$^{-/-}$ and TAC ChGn-2$^{-/-}$. $^{\%\%}P<0.01$ and $^{\%\%\%}P<0.001$ between TAC WT and TAC ChGn-2$^{-/-}$. **D**, Representative images for transversal section of the heart of WT and ChGn-2$^{-/-}$ mice in either sham or TAC group 2 weeks after surgery; bars: 500 μm. **E**, Representative images for Masson trichome staining of the heart in WT and ChGn-2$^{-/-}$ mice in either sham or TAC condition; bars: 200 μm. **F**, Quantification of heart weight normalized to body weight in WT and ChGn-2$^{-/-}$ mice in either sham or TAC condition (n=13 for sham WT, n=10 for sham ChGn-2$^{-/-}$, n=17 for TAC WT, n=15 for TAC ChGn-2$^{-/-}$). **G**, Quantification of heart weight normalized to tibia length in WT and ChGn-2$^{-/-}$ mice in either sham or TAC condition (n=13 for sham WT, n=10 for sham ChGn-2$^{-/-}$, n=17 for TAC WT, n=15 for TAC ChGn-2$^{-/-}$). **H**, Quantification of collagen fibrosis area (%) in the heart of WT and ChGn-2$^{-/-}$ mice in either sham or TAC group 2 weeks after surgery (n=6 for sham WT, n=5 for sham ChGn-2$^{-/-}$, n=8 for TAC WT, n=8 for TAC ChGn-2$^{-/-}$). **I**, Quantitative real time polymerase chain reaction analysis for collagen-1a (Col1a1) in the heart of WT and ChGn-2$^{-/-}$ mice in either sham or TAC group 2 weeks after surgery (n=6 for sham WT, n=5 for sham ChGn-2$^{-/-}$, n=8 for TAC WT, n=8 for TAC ChGn-2$^{-/-}$). **J**, Representative images for TUNEL (terminal deoxynucleotidyl transferase dUTP nick end labeling) and cTnT (cardiac troponin T) double immunofluorescence staining in the heart of WT and ChGn-2$^{-/-}$ mice in either sham or TAC group 2 weeks after surgery. TUNEL and cTnT double-positive apoptotic cells was quantified (n=5 for each group); bars: 50 μm. TUNEL, green; cTnT, red; and 4',6-diamidino-2-28 phenylindole dihydrochloride, blue. **K**, Immunoblotting for caspase-3, cleaved caspase-3 (c.caspase 3), and GAPDH in the heart of WT and ChGn-2$^{-/-}$ mice in either sham or 2 weeks after TAC. Molecular weight (MW) for protein ladders are shown. Apoptosis was assessed by the cleaved caspase-3 expression levels (n=6 for each group). Quantitative data show cleaved caspase 3/total caspase 3 value relative to that in sham WT group. Data represent median and interquartile range. $^{*}P<0.05$, $^{**}P<0.01$, $^{***}P<0.001$, and $^{****}P<0.0001$. Statistical analyses were performed using Kruskal−Wallis test followed by Wilcoxon rank-sum test (F, G, H, I, J, and K). 18s indicates 18s ribosomal RNA; BW, body weight; ChGn-2, chondroitin sulfate N-acetylgalactosaminyltransferase-2; cTnT, cardiac troponin T; DAPI, 4',6-diamidino-2-28 phenylindole dihydrochloride; ChGn-2, chondroitin sulfate N-acetylgalactosaminyltransferase-2; EF, ejection fraction; HW, heart weight; TAC, transverse aortic constriction; TL, tibia length; TUNEL, terminal deoxynucleotidyl transferase dUTP nick end labeling; and WT, wild-type.

We assessed the heart function by serial echocardiography at day 0, 3, 7, 10, and 14 after TAC using male mice. Acute pressure overload continuously deteriorated the LV systolic function in WT mice during the observation period (Figure 2A through 2C). Notably, loss of ChGn-2 caused significant left ventricular dysfunction
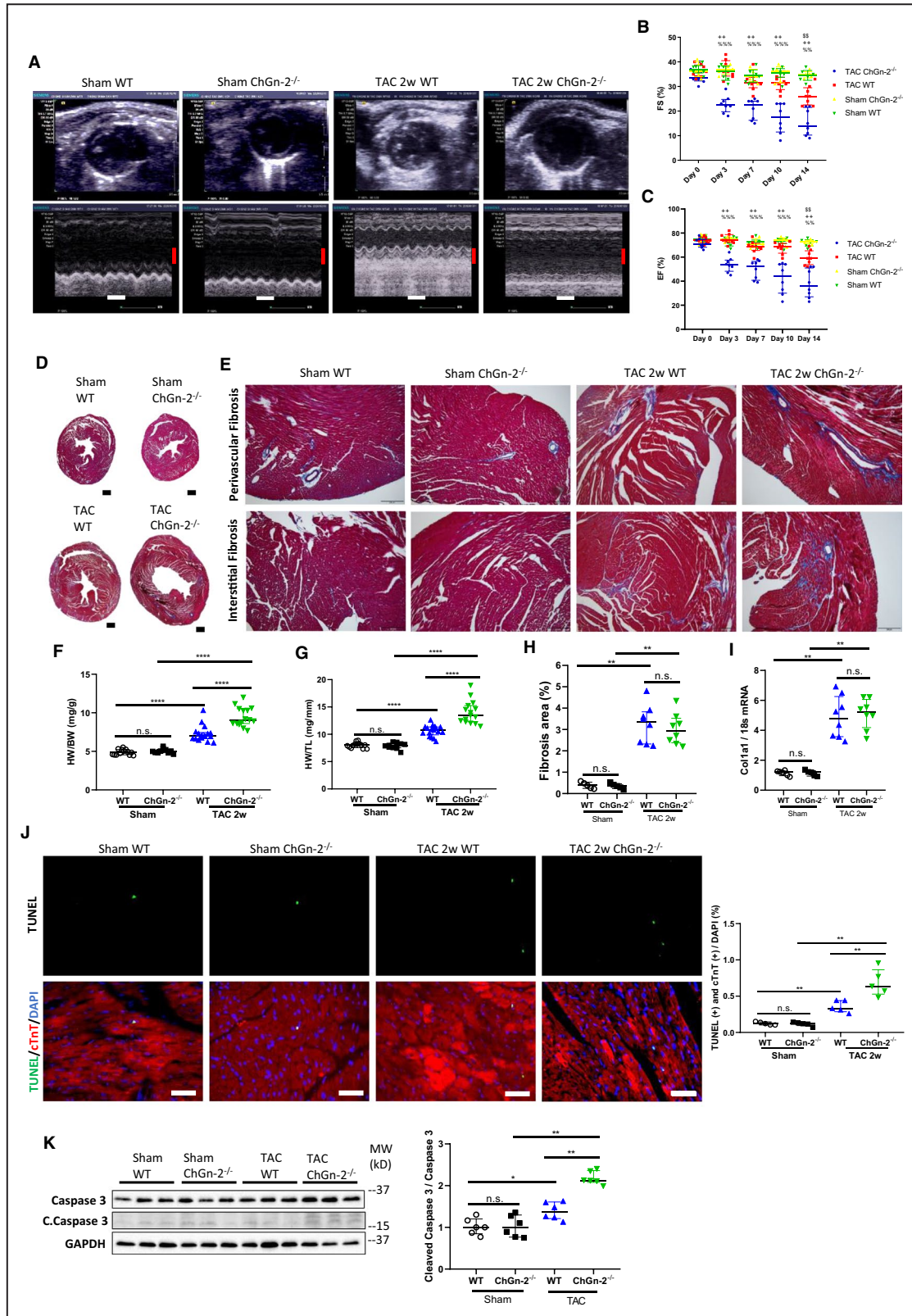
as early as 3 days after TAC, and the worsened LV systolic function remained afterwards in ChGn-2⁻/⁻ mice (Figure 2A through 2C and Figure S1A through S1J). Cardiac hypertrophy assessed by the heart weight was augmented in ChGn-2⁻/⁻ mice (Figure 2D, 2F and 2G),

while cardiac fibrosis, assessed by Masson trichrome staining and collagen mRNA expression, showed no difference between WT and ChGn-2⁻/⁻ mice (Figure 2E, 2H and 2I). Furthermore, ChGn-2⁻/⁻ mice showed less survival rate than that in WT mice after 2 weeks of TAC
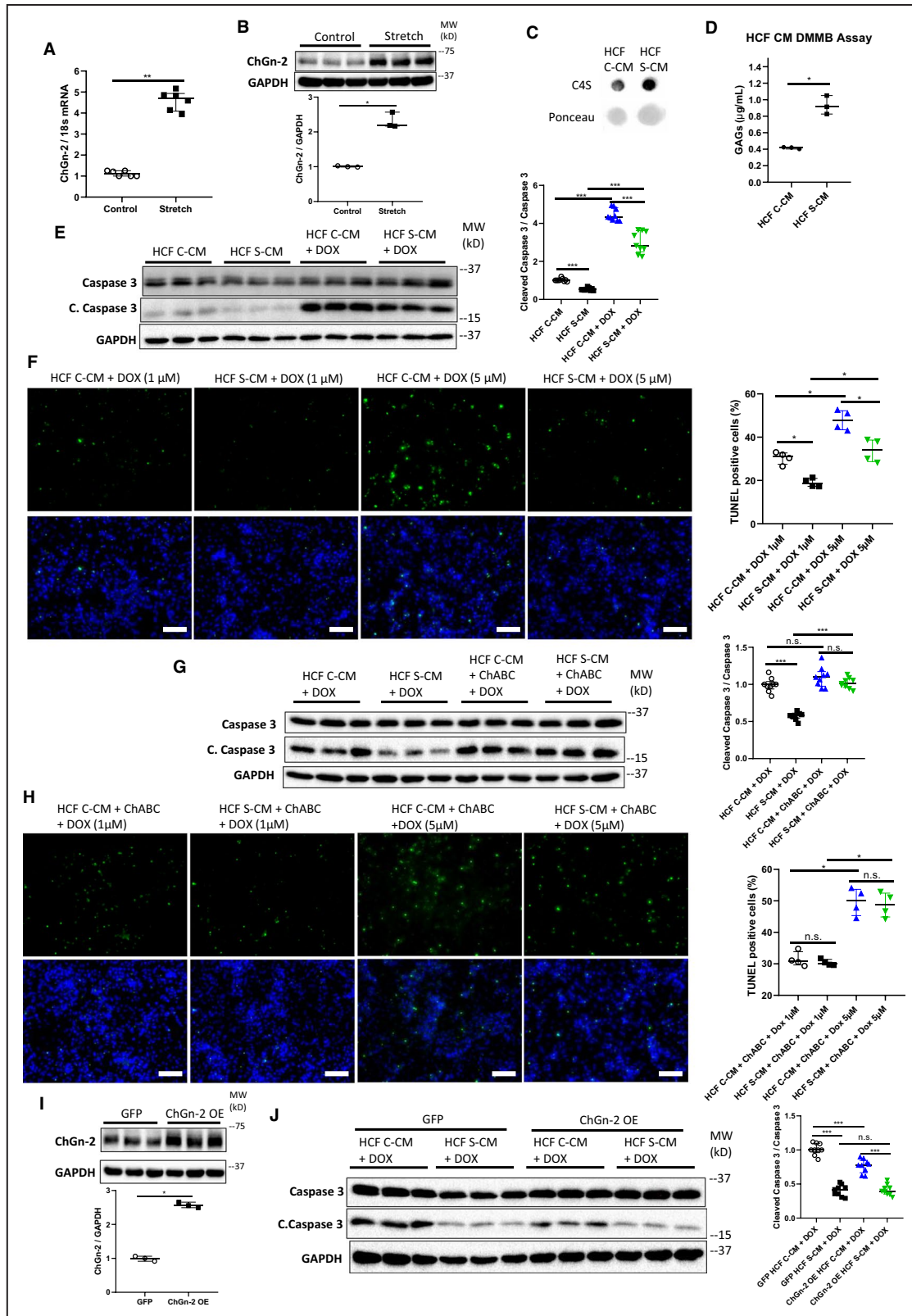
Figure 3.   Mechanical stretch increases glycosaminoglycans production and enhances cardioprotective effects in human cardiac fibroblasts.

A, Quantitative real time polymerase chain reaction analysis for ChGn-2 (chondroitin sulfate N-acetylgalactosaminyltransferase-2) in human cardiac fibroblasts (HCFs) in either control and stretch condition (n=6 for each group). **B**, Immunoblotting for ChGn-2 in HCFs in either control and stretch condition. Molecular weight (MW) for protein ladders are shown. ChGn-2 protein levels were quantified and normalized to GAPDH expression (n=3 for each group). **C**, Dot blot analysis for chondroitin-4-sulfate (C4S) in conditioned medium (CM) derived from HCFs in either control (C-CM) and stretch (S-CM) condition. **D**, Quantification of extracted total glycosaminoglycans in CM derived from HCFs in either C-CM or S-CM (n=3 for each group). **E**, Immunoblotting for caspase-3, cleaved caspase-3 (c.caspase 3), and GAPDH in H9C2 cells treated with CM derived from HCFs in either C-CM or S-CM in the presence or absence of doxorubicin. Molecular weight (MW) for protein ladders are shown. Apoptosis was assessed by the cleaved caspase-3 expression levels normalized to caspase 3 (n=9 for each group). Quantitative data show cleaved caspase 3/total caspase 3 value relative to that in HCF C-CM group. **F**, TUNEL (terminal deoxynucleotidyl transferase dUTP nick end labeling) staining in neonatal rat cardiomyocytes treated with CM derived from HCFs in either C-CM or S-CM in the presence of doxorubicin. TUNEL-positive apoptotic cells were quantified (n=4 for each group); bars: 100 μm. TUNEL, green; and Hoechst, blue. **G**, Immunoblotting for caspase-3, cleaved caspase-3, and GAPDH in H9C2 cells treated with CM derived from HCFs in either C-CM or S-CM in the presence of doxorubicin. Molecular weight (MW) for protein ladders are shown. Some cells were cultured in the CM pretreated with chondroitinase ABC. Apoptosis was assessed by the cleaved caspase-3 expression levels compared with caspase 3 (n=9 for each group). Quantitative data show cleaved caspase 3/total caspase 3 value relative to that in HCF C-CM + doxorubicin group. **H**, TUNEL staining in neonatal rat cardiomyocytes treated with CM derived from HCFs in either C-CM or S-CM in the presence of doxorubicin. Cells were cultured in the CM pretreated with chondroitinase ABC. TUNEL-positive apoptotic cells were quantified (n=4 for each group); bars: 100 μm. TUNEL, green; and Hoechst, blue. **I**, Immunoblotting for ChGn-2 in HCFs infected with retroviruses carrying either green fluorescent protein or ChGn-2 (ChGn-2 overexpression). Molecular weight (MW) for protein ladders are shown. ChGn-2 protein levels were quantified and normalized to GAPDH expression (n=3 for each group). **J**, Immunoblotting for caspase-3, cleaved caspase-3, and GAPDH in H9C2 cells treated with CM derived from HCFs in either C-CM or S-CM in the presence of doxorubicin. Molecular weight (MW) for protein ladders are shown. HCFs infected with retroviruses carrying either green fluorescent protein or ChGn-2 were used. Apoptosis was assessed by the cleaved caspase-3 expression levels compared with caspase 3 (n=9 for each group). Quantitative data show cleaved caspase 3/total caspase 3 value relative to that in green fluorescent protein HCF C-CM + doxorubicin group. Chondroitinase ABC at 10 mIU/mL; doxorubicin at 1 μmol/L were used unless otherwise mentioned. Data represent median and interquartile range. *$P<0.05$, **$P<0.01$, and ***$P<0.001$. Statistical analyses were performed using Wilcoxon rank-sum test (A, B, D, and I) or Kruskal−Wallis test followed by Wilcoxon rank-sum test (E, F, G, H, and J). 18s indicates 18s ribosomal RNA; C-CM, control conditioned medium; ChABC, chondroitinase ABC; ChGn-2, chondroitin sulfate N-acetylgalactosaminyltransferase-2; DMMB, 1,9-dimethylmethylene blue; GFP, green fluorescent protein; HCF, human cardiac fibroblasts; and S-CM, stretch conditioned medium.

(Figure S2). Similar results including the worsened LV systolic dysfunction and the augmented cardiac hypertrophy with similar cardiac fibrosis were observed in female ChGn-2$^{-/-}$ mice compared with those in WT female mice (Figure S3 and S4). Of note, apoptotic cardiomyocyte was more frequently detected in the heart of ChGn-2$^{-/-}$ mice than in WT mice 2 weeks after TAC, suggesting a cardioprotective effect of ChGn-2 and glycosaminoglycans in the acute phase of heart failure (Figure 2J and 2K, Figure S5).

Glycosaminoglycans Derived From Cardiac Fibroblasts Protect Cardiomyocytes From Death

Because cardiac fibroblasts (CFs) are the primary source of CS-GAGs in the heart,[9,38–40] we explored a role of CF-derived glycosaminoglycans in cardiomyocyte death. In overloaded heart, CFs are subjected to mechanical stretch stimuli; therefore, we exposed HCFs to cyclic mechanical stretch in vitro. Mechanical stretch caused significant increase in ChGn-2 expression in HCFs (Figure 3A and 3B). Consistently, mechanical stretch increased the glycosaminoglycans production in HCFs, assessed by the glycosaminoglycans contents in their CM (Figure 3C and 3D). To

explore the role of CFs in cardiomyocyte apoptosis, H9C2 cells and NRCs were incubated in HCF-CM, and apoptosis was induced by doxorubicin treatment. When incubated in CM derived from stretched HCFs, apoptosis was significantly reduced in both H9C2 cells and NRCs (Figure 3E and 3F), suggesting that stretch stimuli enhanced the production/secretion of cardioprotective factors in HCFs. Of note, degradation of glycosaminoglycans using chondroitinase ABC completely abolished the cardioprotective effects of stretched HCFs-CM (Figure 3G and 3H). Furthermore, overexpression of ChGn-2 in HCFs enhanced the cardioprotective effects of their CM even in the absence of the stretch stimuli (Figure 3I and 3J). These results strongly suggest that CFs produce more glycosaminoglycans in association with the enhanced ChGn-2 expression when exposed to stretch stimuli, and these glycosaminoglycans have cardioprotective effects.

ChGn-2 Is Essential for the Stretch-Induced Cardioprotective Function in CFs

We then isolated primary MCFs from WT and ChGn-2$^{-/-}$ mice. Mechanical stretch enhanced ChGn-2 expression, and increased the glycosaminoglycans production in WT MCFs as well as in HCFs (Figure 4A), while ChGn-2$^{-/-}$ MCFs failed to produce more

glycosaminoglycans after stretch stimuli (Figure 4B and 4C). These data indicate that ChGn-2 plays a critical role in the increased glycosaminoglycans production in CFs subjected to mechanical stretch.

Consistent with the results of HCFs, CM derived from stretched WT mouse cardiac fibroblasts (MCFs) showed significant protective effects against apoptosis in H9C2 cells and NRCs (Figure 4D and 4E).
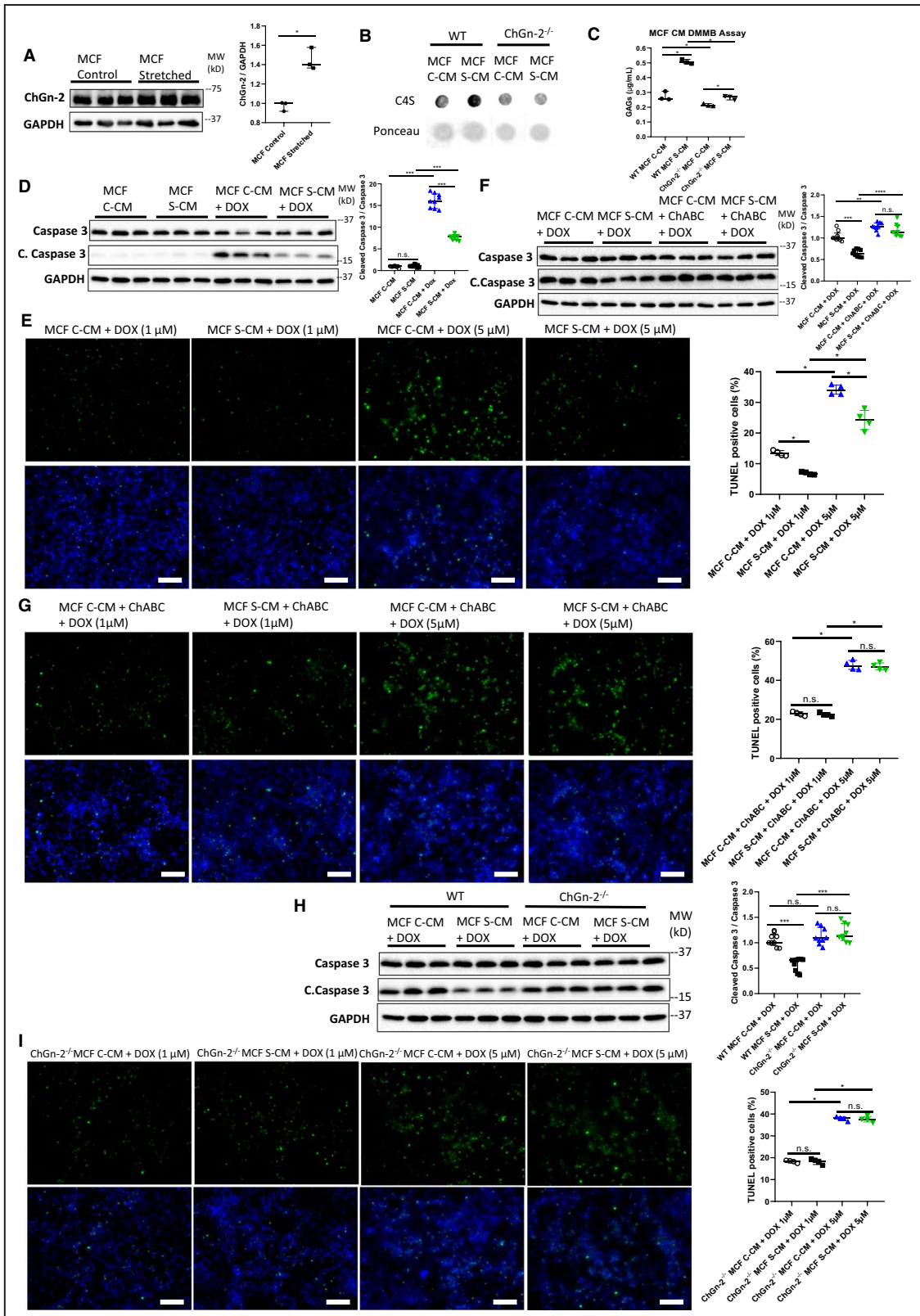
Figure 4. ChGn-2 (chondroitin sulfate N-acetylgalactosaminyltransferase-2) is inevitable for the stretch-mediated cardioprotective effects in mouse cardiac fibroblasts (MCFs).
A, Immunoblotting for ChGn-2 in mouse cardiac fibroblasts (MCFs) in control and stretch conditions. MCFs were isolated from wild-type (WT) mice. ChGn-2 protein levels were quantified and normalized to GAPDH expression (n=3 for each group). **B**, Dot blot analysis for chondroitin-4-sulfate (C4S) in conditioned medium (CM) derived from MCFs in either control (C-CM) or stretch (S-CM) condition. MCFs were isolated from either WT or ChGn-2$^{-/-}$ mice. **C**, Quantification of extracted total glycosaminoglycans in CM derived from MCFs in either control (C-CM) or stretch (S-CM) condition (n=3 for each group). MCFs were isolated from either WT or ChGn-2$^{-/-}$ mice. **D**, Immunoblotting for caspase-3, cleaved caspase-3 (c.caspase 3), and GAPDH in H9C2 cells treated with CM derived from WT-MCFs in either C-CM or S-CM in the presence or absence of doxorubicin. Molecular weight (MW) for protein ladders are shown. Apoptosis was assessed by the cleaved caspase-3 expression levels compared with caspase 3 (n=9 for each group). Quantitative data show cleaved caspase 3/total caspase 3 value relative to that in MCF C-CM group. **E**, TUNEL (terminal deoxynucleotidyl transferase dUTP nick end labeling) staining in neonatal rat cardiomyocytes treated with CM derived from WT-MCFs in either C-CM or S-CM in the presence of doxorubicin. TUNEL-positive apoptotic cells were quantified (n=4 for each group); bars: 100 μm. TUNEL, green; and Hoechst, blue. **F**, Immunoblotting for caspase-3, cleaved caspase-3, and GAPDH in H9C2 cells treated with CM derived from WT-MCFs in either C-CM or S-CM in the presence of doxorubicin. Molecular weight (MW) for protein ladders are shown. Some cells were cultured in the CM pretreated with chondroitinase ABC. Apoptosis was assessed by the cleaved caspase-3 expression levels compared with caspase 3 (n=9 for each group). Quantitative data show cleaved caspase 3/total caspase 3 value relative to that in MCF C-CM + doxorubicin group. **G**, TUNEL staining in neonatal rat cardiomyocytes treated with CM derived from WT-MCFs in either C-CM or S-CM in the presence of doxorubicin. Cells were cultured in the CM pretreated with chondroitinase ABC. TUNEL-positive apoptotic cells were quantified (n=4 for each group); bars: 100 μm. TUNEL, green; and Hoechst, blue. **H**, Immunoblotting for caspase-3, cleaved caspase-3, and GAPDH in H9C2 cells treated with CM derived from MCFs in either C-CM or S-CM condition in the presence of doxorubicin. Molecular weight (MW) for protein ladders are shown. MCFs were isolated from either WT or ChGn-2$^{-/-}$ mice. Apoptosis was assessed by the cleaved caspase-3 expression levels compared with caspase 3 (n=9 for each group). Quantitative data show cleaved caspase 3/total caspase 3 value relative to that in MCF C-CM +doxorubicin group. **I**, TUNEL staining in neonatal rat cardiomyocytes treated with CM derived from ChGn-2$^{-/-}$ MCFs in either C-CM or S-CM in the presence of doxorubicin. TUNEL-positive apoptotic cells were quantified (n=4 for each group); bars: 100 μm. TUNEL, green; and Hoechst, blue. Chondroitinase ABC at 10 mIU/mL; doxorubicin at 1 μmol/L were used for experiments unless otherwise mentioned. Data represent median and interquartile range. *$P<0.05$, **$P<0.01$, and ***$P<0.001$. Statistical analyses were performed using Wilcoxon rank-sum test (A) or Kruskal−Wallis test followed by Wilcoxon rank-sum test (C, D, E, F, G, H, and I). C-CM indicates control conditioned medium; ChABC, chondroitinase ABC; ChGn-2, chondroitin sulfate N-acetylgalactosaminyltransferase-2; DMMB, 1,9-dimethylmethylene blue; MCFs, mouse cardiac fibroblasts; S-CM, stretch conditioned medium; and WT, wild-type.

Degradation of glycosaminoglycans by chondroitinase ABC completely abrogated the cardioprotective effects of stretched MCFs-CM, indicating the critical role of glycosaminoglycans in the stretch-mediated cardioprotective effects of in CFs (Figure 4F and 4G). Notably, cardioprotective effects of stretched MCF-CM disappeared in ChGn-2$^{-/-}$ MCFs (Figure 4H and 4I). Moreover, retrovirus-mediated overexpression of ChGn-2 enhanced the cardioprotective effects of MCF-CM in both WT and ChGn-2$^{-/-}$ MCFs even in the absence of mechanical stretch stimuli (Figure 5A through 5F). These data collectively indicate that mechanical stretch enhances ChGn-2 expression, which promotes glycosaminoglycans elongation, in CFs, and the increased glycosaminoglycans protect cardiomyocytes from death.

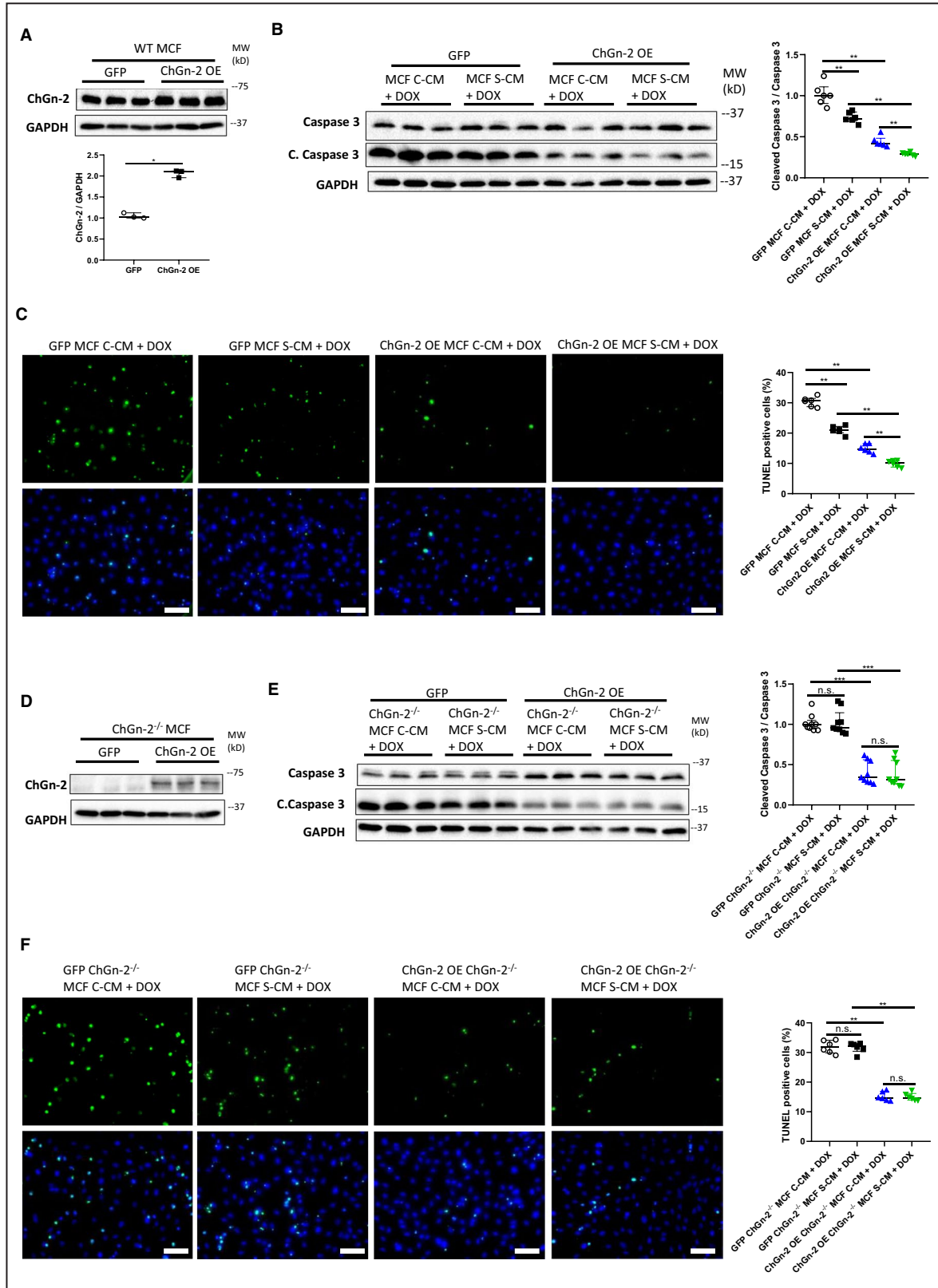## Chondroitin Sulfate A Protects Cardiomyocyte From Death Via CD44

To further analyze the cardioprotective role of CS-GAG, we examined the effects of purified chondroitin sulfate A (CS-A), which is one of the major glycosaminoglycans produced by CFs,[9] in cardiomyocyte apoptosis. Treatment with CS-A attenuated the apoptosis in H9C2 cells in association with preserved Akt activity after doxorubicin administration

(Figure 6A through 6C). CS-A also inhibited cardiomyocyte death in NRCs (Figure 6D). These data strongly suggest the direct inhibitory effect of CS-A on cardiomyocyte death. Because CS-A inhibited the cell death in association with preserved Akt activity, we examined whether PI3K/Akt pathway is implicated in the CS-A–mediated cardioprotection. Inhibition of PI3K/Akt pathway by LY294002 abolished the reduced apoptosis in H9C2 cells treated with CS-A, indicating that PI3K/Akt pathway is critically involved in the CS-A–mediated cardioprotection (Figure 6E through 6G).

Cell surface glycoprotein CD44 has been reported as a receptor for CS-GAGs in hematopoietic cell lines,[41] rat chondrosarcoma cells,[42] human pancreatic adenocarcinoma cells,[43] and human lung cancer cells.[44] Also, it has been reported that CD44 activate PI3K/Akt pathway in lymphocytes and many types of cancer cells[45–51] to promote those cells survival and proliferation. We therefore explored whether CD44 is involved in the CS-GAG-mediated cardioprotection. Blocking CD44 by anti-CD44 antibody diminished the inhibitory effects of CS-A on apoptosis in H9C2 cells in conjunction with abrogating the Akt activity preservation after doxorubicin treatment (Figure 6H through 6J). Blocking CD44 also abolished the cardioprotective effects of CS-A in NRCs (Figure 6K).

Combination treatment of CD44ab and LY294002 did not show additive effects on reduction of the CS-A-mediated anti-apoptosis effect compared with each of the compound, suggesting that CD44 and PI3K/Akt work in the same pathway (Figure S6). These data collectively suggest that CS-GAGs protect

Figure 5. Overexpression of ChGn-2 augments the cardioprotective effects in mouse cardiac fibroblasts (MCFs).
A, Immunoblotting for ChGn-2 (chondroitin sulfate N-acetylgalactosaminyltransferase-2) in wild-type (WT) mouse cardiac fibroblasts (MCFs) infected with retroviruses carrying either green fluorescent protein (GFP) or ChGn-2 (ChGn-2 overexpression). Molecular weight (MW) for protein ladders are shown. ChGn-2 protein levels were quantified and normalized to GAPDH expression (n=3 for each group). **B**, Immunoblotting for caspase-3, cleaved caspase-3 (c.caspase 3), and GAPDH in H9C2 cells treated with conditioned medium (CM) derived from WT MCFs in either control (C-CM) or stretch (S-CM) condition in the presence of doxorubicin. Molecular weight (MW) for protein ladders are shown. WT MCFs infected with retroviruses carrying either GFP or ChGn-2 (ChGn-2 overexpression) were used. Apoptosis was assessed by the cleaved caspase-3 expression levels compared with caspase 3 (n=6 for each group). Quantitative data show cleaved caspase 3/total caspase 3 value relative to that in GFP MCF C-CM + doxorubicin group. **C**, TUNEL (terminal deoxynucleotidyl transferase dUTP nick end labeling) staining in in H9C2 cells treated with CM derived from WT MCFs in either C-CM or S-CM in the presence of doxorubicin. WT MCFs infected with retroviruses carrying either GFP or ChGn-2 (ChGn-2 overexpression) were used. TUNEL-positive apoptotic cells were quantified (n=6 for each group); bars: 100 μm. TUNEL, green; and Hoechst, blue. **D**, Immunoblotting for ChGn-2 in ChGn-2$^{-/-}$ MCFs infected with retroviruses carrying either GFP or ChGn-2 (ChGn-2 overexpression). Molecular weight (MW) for protein ladders are shown. **E**, Immunoblotting for caspase-3, cleaved caspase-3, and GAPDH in H9C2 cells treated with CM derived from ChGn-2$^{-/-}$ MCFs in either C-CM or S-CM in the presence of doxorubicin. Molecular weight (MW) for protein ladders are shown. ChGn-2$^{-/-}$ MCFs infected with retroviruses carrying either GFP or ChGn-2 (ChGn-2 overexpression) were used. Apoptosis was assessed by the cleaved caspase-3 expression levels (n=9 for each group). Quantitative data show cleaved caspase 3/total caspase 3 value relative to that in GFP ChGn-2$^{-/-}$ MCF C-CM + doxorubicin group. **F**, TUNEL staining in H9C2 cells treated with CM derived from ChGn-2$^{-/-}$ MCFs in either C-CM or S-CM in the presence of doxorubicin. ChGn-2$^{-/-}$ MCFs infected with retroviruses carrying either GFP or ChGn-2 (ChGn-2 OE) were used. TUNEL-positive apoptotic cells were quantified (n=6 for each group); bars: 100 μm. TUNEL, green; and Hoechst, blue. Doxorubicin was used at 1 μmol/L. Data represent median and interquartile range. *$P<0.05$, **$P<0.01$, and ***$P<0.001$. Statistical analyses were performed using Wilcoxon rank-sum test (A) or Kruskal–Wallis test followed by Wilcoxon rank-sum test (B, C, E, and F). C-CM indicates control conditioned medium; ChABC, chondroitinase ABC; ChGn-2, chondroitin sulfate N-acetylgalactosaminyltransferase-2; GFP, green fluorescent protein; MCFs, mouse cardiac fibroblasts; S-CM, stretch conditioned medium; and WT, wild-type.

cardiomyocytes from death directly via CD44-PI3K/AKT axis.

CS-A Inhibits Cardiomyocyte Death by Activating Insulin-Like Growth Factor-1-1

CS-GAGs binds to various soluble factors including proteases, cytokines, and growth factors to modulate their biological functions.[5,15,52–59] Binding to CS-GAGs leads to efficient accumulation and/or retention of soluble factors at specific sites, which largely promotes their biological functions.[60–64] CFs produce various cardioprotective growth factors. We found that stretch stimuli substantially increased insulin-like growth factor-1 (IGF-1) expression in HCFs (Figure 7A), and that stretched HCF-CM showed higher IGF-1 concentration than in control HCF-CM (Figure S7). Therefore, we explored a possible interaction between CS-GAGs and IGF-1. We first analyzed whether CS-A binds to IGF-1. Cell culture dishes were coated with CS-A, followed by incubation with IGF-1. After washing out the unbound IGF-1, H9C2 cells were plated onto the dishes, and the effect of IGF-1 (bound to CS-A coating) was analyzed (Figure S8). CS-A coating caused significant retention of IGF-1, which induced atrial natriuretic peptide and brain natriuretic peptide expression in H9C2 cells cultured on the dishes (Figure 7B). Notably, digestion of CS-GAG using chondroitinase ABC abolished the retention of IGF-1 (Figure 7B). IGF-1 bound to CS-A-coated dish sufficiently activated Akt and inhibited the apoptosis in H9C2 cells cultured on the dishes in serum free medium containing doxorubicin, as well

as the control group (100 ng/mL IGF-1 directly added into the culture medium) (Figure 7C).

We then assessed whether binding to CS-A affects the biological function of IGF-1. Addition of IGF-1 in the medium strongly activated Akt, and inhibited doxorubicin-induced apoptosis in H9C2 cells (Figure 7D). Of note, treatment with IGF-1 in the presence of CS-A showed synergistic, rather than additive, cardioprotective effects, suggesting that interaction with CS-A might enhance IGF-1 cardioprotective functions (Figure 7D). These data indicate that CS-GAGs protect cardiomyocyte from death via dual pathway; direct pathway through CD44 and indirect pathway through binding to and activating IGF-1 (Figure S9).

To investigate which pathway is more important for CS-GAG to protect cardiomyocyte, we assessed the effects of CD44 blockade on the cardioprotective effects of CM derived from stretched MCFs. CS-GAGs chains and IGF-1, which are rich in the CM of the stretched MCFs, should activate both direct and indirect pathway of CS-GAGs to protect cardiomyocyte. In this experiment, we blocked the direct pathway through CD44 using CD44 antibody, and examined the role of remaining indirect pathway in cardioprotective effects mediated by CS-GAGs. Blocking CD44 showed no significant effects on the cardioprotective effects of CM derived from stretched MCFs in H9C2 cells (Figure 7E), suggesting the minimal role of direct pathway in the CS-GAGs-mediated cardioprotection. In contrast, cardioprotective effects of stretched MCFs-derived CM were significantly attenuated by CD44 blockade in NRCs, indicating a crucial role of direct

pathway for CS-GAGs to protect cardiomyocytes (Figure 7F). These data suggest that both direct and indirect pathway is important in CS-GAGs-mediated cardioprotection, although indirect pathway appeared to play a major role.

DISCUSSION

In this study, we revealed a cardioprotective role of ChGn-2 and CS-GAGs in the progression of heart failure using acute pressure overload model. Pressure
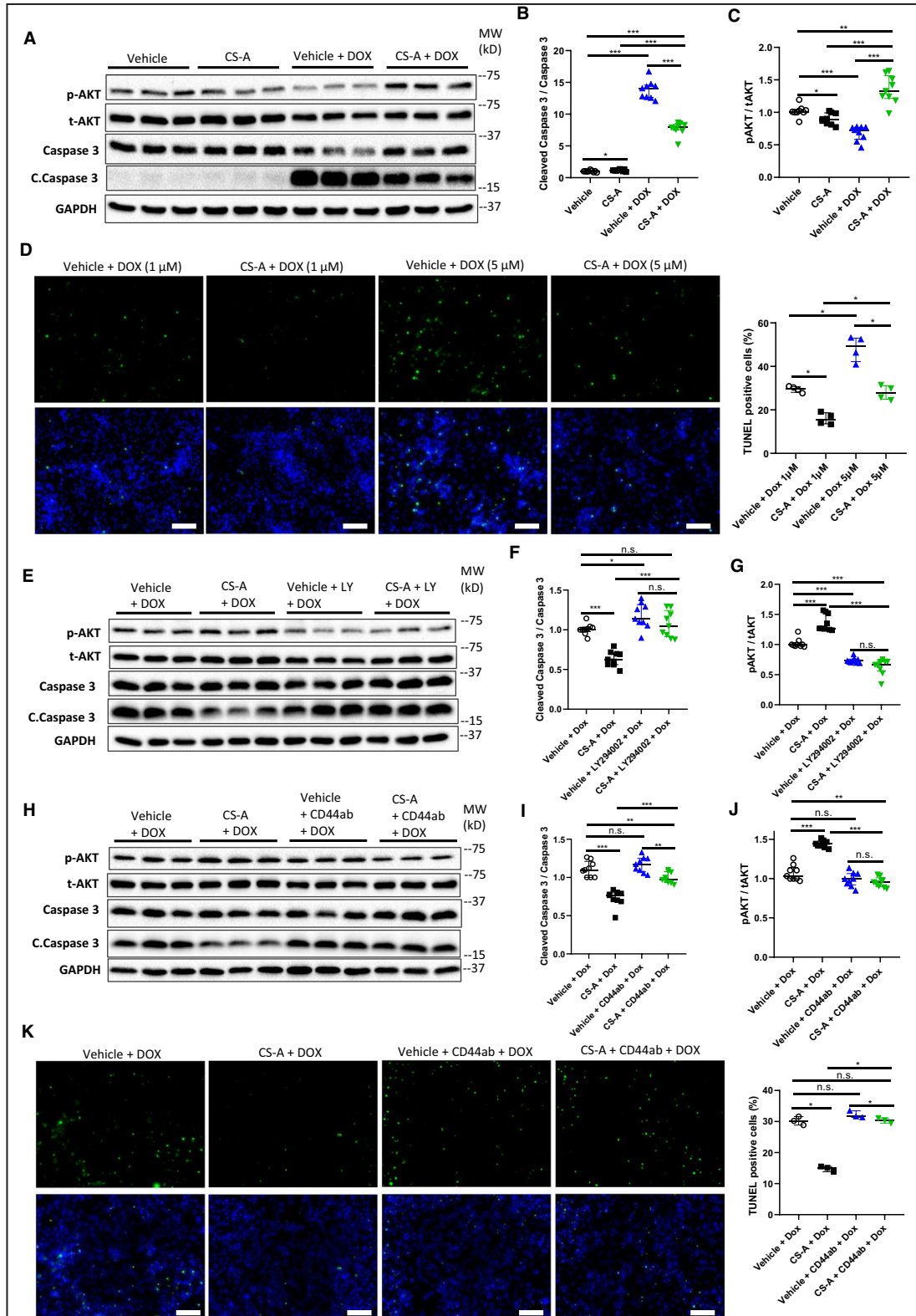
Figure 6.   Purified chondroitin sulfate A (CS-A) shows cardioprotective effects.
A, Immunoblotting for caspase-3, cleaved caspase-3 (c.caspase 3), phospho-AKT (p-AKT), total-AKT (t-AKT), and GAPDH in H9C2 cells treated with either vehicle or CS-A in the presence or absence of doxorubicin. Molecular weight (MW) for protein ladders are shown. **B**, Apoptosis was assessed by the cleaved caspase-3 (c.caspase 3) expression levels compared with caspase 3 (n=9 for each group). Quantitative data show cleaved caspase 3/total caspase 3 value relative to that in vehicle group. **C**, Akt activity was assessed by quantification of p-AKT compared with t-AKT (n=9 for each group). Quantitative data show p-AKT/t-AKT value relative to that in vehicle group. **D**, TUNEL (terminal deoxynucleotidyl transferase dUTP nick end labeling) staining in neonatal rat cardiomyocytes treated with either vehicle or CS-A in the presence of doxorubicin. TUNEL-positive apoptotic cells were quantified (n=4 for each group); bars: 100 μm. TUNEL, green; and Hoechst, blue. **E**, Immunoblotting for caspase-3, cleaved caspase-3, p-AKT, t-AKT, and GAPDH in H9C2 cells treated with either vehicle or CS-A in the presence of doxorubicin. Molecular weight (MW) for protein ladders are shown. Some cells were treated with phosphoinositide 3-kinases inhibitor, LY294002 (LY). **F**, Apoptosis was assessed by the cleaved caspase-3 expression levels compared with caspase 3 (n=9 for each group). Quantitative data show cleaved caspase 3/total caspase 3 value relative to that in vehicle + doxorubicin group. **G**, Akt activity was assessed by quantification of p-AKT compared with t-AKT (n=9 for each group). Quantitative data show p-AKT/t-AKT value relative to that in vehicle + doxorubicin group. **H**, Immunoblotting for caspase-3, cleaved caspase-3, p-AKT t-AKT, and GAPDH in H9C2 cells treated with either vehicle or CS-A in the presence of doxorubicin. Molecular weight (MW) for protein ladders are shown. Some cells were treated with anti-CD44 antibody (CD44ab). **I**, Apoptosis was assessed by the cleaved caspase-3 expression levels compared with caspase 3 (n=9 for each group). Quantitative data show cleaved caspase 3/total caspase 3 value relative to that in vehicle + doxorubicin group. **J**, Akt activity was assessed by quantification of p-AKT compared with t-AKT (n=9 for each group). Quantitative data show p-AKT/t-AKT value relative to that in vehicle + doxorubicin group. **K**, TUNEL staining in neonatal rat cardiomyocytes treated with either vehicle or CS-A in the presence of doxorubicin. Some cells were treated with anti-CD44 antibody (CD44ab). TUNEL-positive apoptotic cells were quantified (n=3 for each group). Bars: 100 μm. TUNEL, green; and Hoechst, blue. CS-A at 500 μg/mL; LY294002 at 25 μmol/L; CD44ab at 1: 200 dilution; doxorubicin at 1 μmol/L were used for experiments unless otherwise mentioned. Data represent median and interquartile range. *$P<0.05$, **$P<0.01$, and ***$P<0.001$. n.s., not significant. Statistical analyses were performed using Kruskal–Wallis test followed by Wilcoxon rank-sum test **(B, C, D, F, G, I, J, and K)**. CS-A indicates chondroitin sulfate A; LY, LY294002; pAKT, phospho-AKT; tAKT, total-AKT; and TUNEL, terminal deoxynucleotidyl transferase dUTP nick end labeling.

overload results in cardiac hypertrophy and fibrosis that is characterized with accumulation of collagen and glycosaminoglycans in interstitial and perivascular in the heart.[23,65–67] This condition mimics systemic hypertension which is associated with progressive interstitial and perivascular deposition of ECM proteins that increase myocardial stiffness and cause diastolic dysfunction.[68,69]

CFs are a primary source of chondroitin sulfate proteoglycans in the heart.[9,38–40] Also, CFs have been shown to interact with cardiomyocyte via direct contact and indirect pathway through secreted factors. This complex interaction influences cardiomyocyte phenotype such as hypertrophy, contractility, survival, and differentiation.[70–74] In overloaded heart, CFs are subjected to mechanical stretch, which has been reported to induce secretion of growth factors, collagens, proteoglycans, and micro RNA containing exosomes.[33,75–79] Our data revealed mechanistic insights in a facet of the CFs-cardiomyocytes interaction under pathologic condition. Increased workload induces ChGn-2 expression in CFs through the mechanical stretch, leading to the more production of CS-GAGs and cardioprotective growth factors including IGF-1. These CS-GAGs and IGF-1 show synergistic cardioprotective effects to inhibit the progression of heart failure at least in an acute phase. We found that various cardioprotective factors such as basic fibroblast growth factor, platelet-derived growth factor subunit A and granulocyte-colony stimulating factor were increased in CFs subjected to mechanical stretch, while we examined only a role of IGF-1 in the

cardioprotective effects mediated through CS-GAGs. Potential role of other factors need to be analyzed in future experiments. Also, there is a caveat to be noted in our study. Because fibroblast cells will transdifferentiate into myofibroblasts when cultured in polystyrene plates and passaged several times,[31] some of CFs in our experiments might have transdifferentiated into myofibroblasts that show cellular responses different from those in CFs.

Previous findings have described interaction of chondroitin sulfate proteoglycans by its CS-GAGs chains with numerous soluble ligands and receptors. These interactions cause indirect enhancement or inhibition of signaling pathways by augmentation of soluble factors bioavailability, enforcement of those soluble ligands binding to its receptors or blockade have been described.[56–59,80–83] On the other hand, much less is known about the direct modulation of signaling pathway by CS-GAGs. Our data strongly suggest that CS-GAGs have direct cardioprotective effects through CD44/Akt axis, although further analyses are required to answer questions; how CS-GAGs interact with CD44?, Is there specificity for chondroitin sulfate proteoglycans in this CS-GAG-CD44 interaction?, how this interaction affects CD44 functions?, and how CD44 modulates Akt activity?

Previous research showed a detrimental role of CS-GAGs in the development of heart failure.[9] Authors demonstrated the excess accumulation of CS-GAGs in the human failing heart of end-stage cardiomyopathy. Subsequently, they showed that treatment with rhASB (chondroitin-4-sulfate-specific sulfatase)

starting at 2 weeks after TAC improved the LV systolic function assessed at 8 weeks after TAC in rats. Finally, they demonstrated that CS-GAGs binds to TNF-α, and potentiates TNF-α-induced inflammation.

Considering an important role of chronic inflammation in the development of heart failure, these data suggest a detrimental role of excess CS-GAGs in chronic heart failure by augmenting cardiac inflammation. In
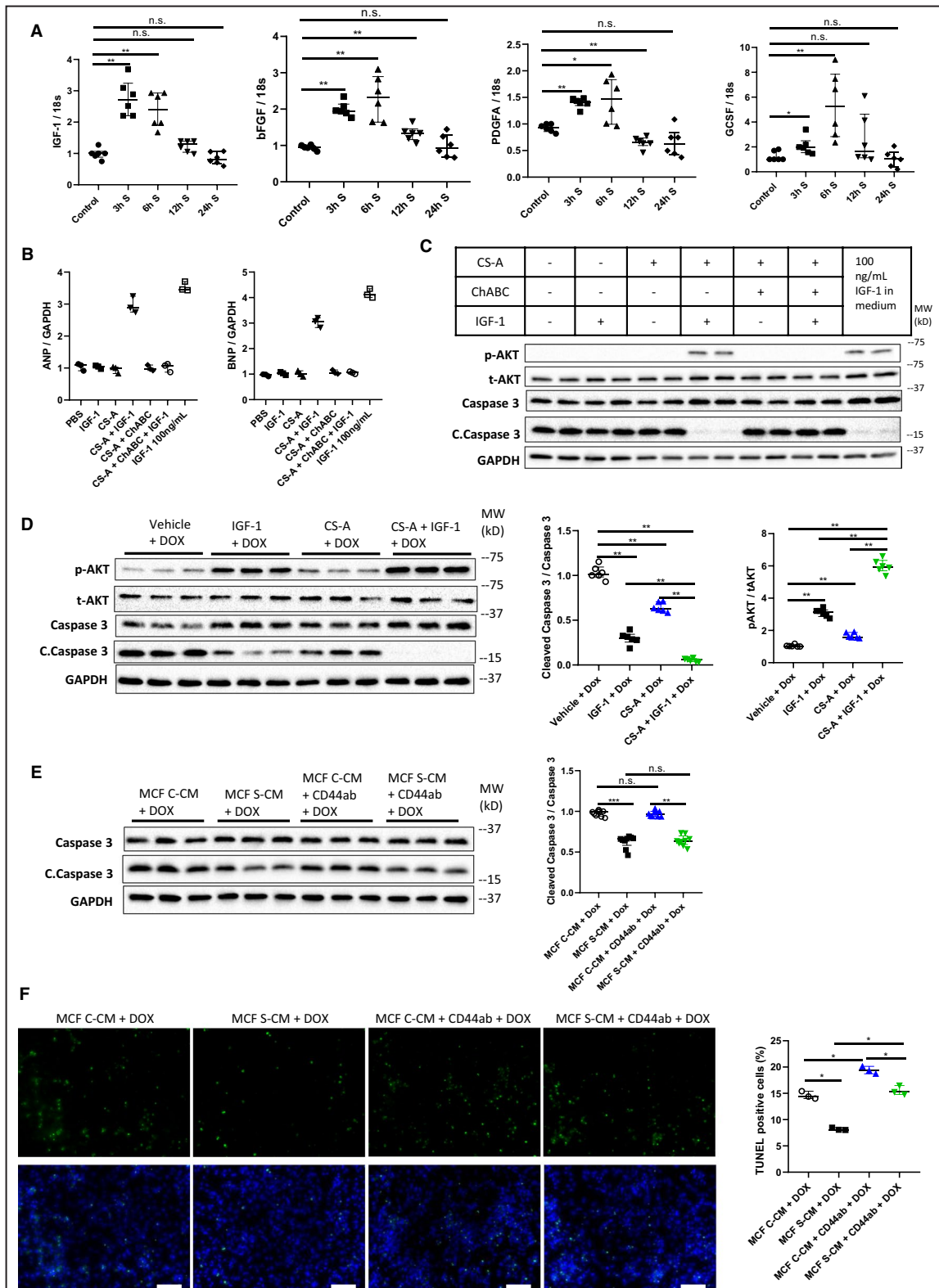
Figure 7. Chondroiton sulfate A (CS-A) binds to insulin-like growth factor 1 (IGF-1) and augments its cardioprotective effects. **A**, Quantitative real time polymerase chain reaction analysis for insulin-like growth factor 1, basic fibroblast growth factor, platelet derived growth factor subunit A, and granulocyte colony-stimulating factor in human cardiac fibroblasts in either control or stretch condition (n=6 for each group). Cells were given stretch stimuli for 3h S, 6h S, 12h S, and 24h S, respectively. **B**, Culture plates were coated with CS-A in the presence or absence of chondroitinase ABC. Negative control plates were prepared by incubating with PBS. Subsequently, plates were incubated with 100 ng/mL IGF-1 for 2 hours at 37 °C, followed by washing with PBS. H9C2 cells were then seeded onto the plates, and incubated for 24 hours. RNAs were extracted from cells, and atrial natriuretic peptide and brain natriuretic peptide mRNA expression was quantitatively analyzed with GAPDH as normalization (n=3 each). As a positive control, cells were seeded on non-coated plate (without incubation with IGF-1), and 100 ng/mL IGF-1 was added in the culture medium at the time of cell seeding. For detailed experimental procedures, see Figure S8. **C**, Culture plates were coated with CS-A in the presence or absence of chondroitinase ABC. Negative control plates were prepared by incubating with PBS. Subsequently, plates were incubated with 100 ng/mL IGF-1 for 2 hours at 37 °C, followed by washing with PBS. H9C2 cells were then seeded onto the plates, and incubated for 24 hours. Then, the cells were treated with doxorubicin for 3 hours (see Figure S8 for detailed experimental procedures). Caspase-3, cleaved caspase-3 (c.caspase 3), phospho-AKT, total-AKT, and GAPDH expressions were analyzed by immunoblotting. Molecular weight (MW) for protein ladders are shown. As a positive control, cells were seeded on non-coated plate (without incubation with IGF-1), and 100 ng/mL IGF-1 was added in the culture medium at the time of cell seeding. **D**, Immunoblotting for caspase-3, cleaved caspase-3, phospho-AKT, total-AKT, and GAPDH in H9C2 cells treated with either vehicle, IGF-1, CS-A, or IGF-1+CS-A in the presence of doxorubicin. Apoptosis was assessed by the cleaved caspase-3 expression levels compared with caspase 3 (n=6 for each group). AKT activity was also assessed by quantification of phospho-AKT compared with total-AKT (n=6 for each group). Quantitative data show cleaved caspase 3/total caspase 3 and phospho-AKT/total-AKT values relative to those in vehicle + doxorubicin group. **E**, Immunoblotting for caspase-3, cleaved caspase-3, and GAPDH in H9C2 cells treated with conditioned medium (CM) derived from wild-type (WT) mouse cardiac fibroblasts in either control-CM or stretch-CM in the presence of doxorubicin. Molecular weight (MW) for protein ladders are shown. Some cells were treated with anti-CD44 antibody (CD44ab). Apoptosis was assessed by the cleaved caspase-3 expression levels compared with caspase 3 (n=9 for each group). Quantitative data show cleaved caspase 3/total caspase 3 value relative to that in mouse cardiac fibroblasts control-CM + doxorubicin group. **F**, TUNEL (terminal deoxynucleotidyl transferase dUTP nick end labeling) staining in neonatal rat cardiomyocytes treated with CM derived from WT- mouse cardiac fibroblasts in either control-CM or stretch-CM condition in the presence of doxorubicin. Some cells were treated with anti-CD44 antibody (CD44ab). TUNEL-positive apoptotic cells were quantified (n=3 for each group); bars: 100 µm. TUNEL, green; and Hoechst; blue. CS-A at 500 µg/mL; IGF-1 at 10 ng/mL; CD44ab at 1: 200 dilution; doxorubicin at 1 µmol/L (**D through F**) were used for experiments. Data represent median and interquartile range. *P<0.05, **P<0.01, and ***P<0.001. n.s., not significant. Statistical analyses were performed using Kruskal−Wallis test followed by Wilcoxon rank-sum test (**D through F**). 18s indicates 18s ribosomal RNA; ANP, atrial natriuretic peptide; bFGF, basic fibroblast growth factor; BNP, brain natriuretic peptide; C-CM, control conditioned medium; ChABC, chondroitinase ABC; CS-A, chondroitin sulfate A; GCSF, granulocyte colony-stimulating factor; IGF-1, insulin-like growth factor 1; MCFs, mouse cardiac fibroblasts; pAKT, phospho-AKT; PDGFA, platelet derived growth factor subunit A; S-CM, stretch conditioned medium; and tAKT, total-AKT.

contrast, our data showed that insufficient CS-GAGs production (because of loss of ChGn-2) deteriorated LV systolic function as early as 3 days after TAC in mice. Furthermore, we demonstrated the cardioprotective role of CS-GAGs in doxorubicin-mediated acute cardiomyocyte injury model. These data strongly suggest that sufficient amount of CS-GAGs is required for cardiomyocyte to resist the acute injury stress. It is not clear whether less production and/or accumulation of CS-GAGs in ChGn-2$^{-/-}$ mice is beneficial for cardiac function at chronic phase (for example, 8 weeks after TAC). Considering the remarkable reduction of LV systolic function in ChGn-2$^{-/-}$ mice after TAC, we presume that worsened cardiac function attributable to insufficient CS-GAGs production at acute phase might not be overcome even though less CS-GAGs might lead to reduced inflammation at chronic phase. Increased production of CS-GAGs in CFs subjected to mechanical stretch might be an adaptive response to resist the acute pressure overload stress, while continuous CS-GAGs-overproduction may cause maladaptation. Investigating an effect of exogenously injected CS-A in mice will provide important information to further confirm the cardioprotective effects of CS-GAGs. Because CS-GAGs appeared to have biphasic effects on cardiac function and remodeling in heart failure, careful consideration and stage-dependent strategies are needed for the CS-GAGs−targeted therapy against heart failure.

Disclosures

None.

Supplemental Material

Tables S1–S2
Figures S1–S9

REFERENCES

1. Christensen G, Herum KM, Lunde IG. Sweet, yet underappreciated: proteoglycans and extracellular matrix remodeling in heart disease. *Matrix Biol*. 2019;76:286–299. doi: 10.1016/j.matbio.2018.01.001

2. Wang X, Lu Y, Xie Y, Shen J, Xiang M. Emerging roles of proteoglycans in cardiac remodeling. *Int J Cardiol*. 2019;278:192–198. doi: 10.1016/j.ijcard.2018.11.125

3. Rienks M, Papageorgiou AP, Frangogiannis NG, Heymans S. Myocardial extracellular matrix: an ever-changing and diverse entity. *Circ Res*. 2014;114:872–888. doi: 10.1161/CIRCRESAHA.114.302533

4. Schaefer L, Schaefer RM. Proteoglycans: from structural compounds to signaling molecules. *Cell Tissue Res*. 2010;339:237–246. doi: 10.1007/s00441-009-0821-y

5. Kitagawa H. Using sugar remodeling to study chondroitin sulfate function. *Biol Pharm Bull*. 2014;37:1705–1712. doi: 10.1248/bpb.b14-00613

6. Zuo J, Neubauer D, Graham J, Krekoski CA, Ferguson TA, Muir D. Regeneration of axons after nerve transection repair is enhanced by degradation of chondroitin sulfate proteoglycan. *Exp Neurol*. 2002;176:221–228. doi: 10.1006/exnr.2002.7922

7. Jones LL, Sajed D, Tuszynski MH. Axonal regeneration through regions of chondroitin sulfate proteoglycan deposition after spinal cord injury: a balance of permissiveness and inhibition. *J Neurosci*. 2003;23:9276–9288. doi: 10.1523/jneurosci.23-28-09276.2003

8. Dyck S, Kataria H, Alizadeh A, Santhosh KT, Lang B, Silver J, Karimi-Abdolrezaee S. Perturbing chondroitin sulfate proteoglycan signaling through LAR and PTPσ receptors promotes a beneficial inflammatory response following spinal cord injury. *J Neuroinflammation*. 2018;15:90. mo10.1186/s12974-018-1128-2

9. Zhao R-R, Ackers-Johnson M, Stenzig J, Chen C, Ding T, Zhou Y, Wang P, Ng SL, Li PY, Teo G, et al. Targeting chondroitin sulfate glycosaminoglycans to treat cardiac fibrosis in pathological remodeling. *Circulation*. 2018;137:2497–2513. doi: 10.1161/CIRCULATIONAHA.117.030353

10. Peal DS, Burns CG, Macrae CA, Milan D. Chondroitin sulfate expression is required for cardiac atrioventricular canal formation. *Dev Dyn*. 2009;238:3103–3110. doi: 10.1002/dvdy.22154

11. Prinz RD, Willis CM, van Kuppevelt TH, Klüppel M. Biphasic role of chondroitin sulfate in cardiac differentiation of embryonic stem cells through inhibition of Wnt/β-catenin signaling. *PLoS One*. 2014;9:e92381. doi: 10.1371/journal.pone.0092381

12. Melgar-Lesmes P, Garcia-Polite F, Del-Rey-Puech P, Rosas E, Dreyfuss JL, Montell E, Vergés J, Edelman ER, Balcells M. Treatment with chondroitin sulfate to modulate inflammation and atherogenesis in obesity. *Atherosclerosis*. 2016;245:82–87. doi: 10.1016/j.atherosclerosis.2015.12.016

13. Martínez-Calatrava MJ, Largo R, Herrero-Beaumont G. Improvement of experimental accelerated atherosclerosis by chondroitin sulphate. *Osteoarthr Cartil*. 2010;18:S12–S16. doi: 10.1016/j.joca.2010.01.014

14. Zinellu E, Lepedda AJ, Cigliano A, Pisanu S, Zinellu A, Carru C, Bacciu PP, Piredda F, Guarino A, Spirito R, et al. Association between human plasma chondroitin sulfate isomers and carotid atherosclerotic plaques. *Biochem Res Int*. 2012;2012:1–6. doi: 10.1155/2012/281284

15. Mikami T, Kitagawa H. Biosynthesis and function of chondroitin sulfate. *Biochim Biophys Acta - Gen Subj*. 2013;1830:4719–4733. doi: 10.1016/j.bbagen.2013.06.006

16. Izumikawa T, Okuura Y, Koike T, Sakoda N, Kitagawa H. Chondroitin 4-O-sulfotransferase-1 regulates the chain length of chondroitin sulfate in co-operation with chondroitin N- acetylgalactosaminyltransferase-2. *Biochem J*. 2011;434:321–331. doi: 10.1042/BJ20101456

17. Sato T, Gotoh M, Kiyohara K, Akashima T, Iwasaki H, Kameyama A, Mochizuki H, Yada T, Inaba N, Togayachi A, et al. Differential roles of two N-acetylgalactosaminyltransferases, CSGalNAcT-1, and a novel enzyme, CSGalNAcT-2. Initiation and elongation in synthesis of chondroitin sulfate. *J Biol Chem*. 2003;278:3063–3071. doi: 10.1074/jbc.M208886200

18. Adhikara IM, Yagi K, Mayasari DS, Ikeda K, Kitagawa H, Miyata O, Igarashi M, Hatakeyama K, Asada Y, Hirata K-I, et al. Chondroitin sulfate N-acetylgalactosaminyltransferase-2 deletion alleviates lipoprotein retention in early atherosclerosis and attenuates aortic smooth muscle cell migration. *Biochem Biophys Res Commun*. 2019;509:89–95. doi: 10.1016/j.bbrc.2018.12.068

19. Adhikara IM, Yagi K, Mayasari DS, Suzuki Y, Ikeda K, Ryanto GRT, Sasaki N, Rikitake Y, Nadanaka S, Kitagawa H, et al. Chondroitin sulfate N -acetylgalactosaminyltransferase-2 impacts foam cell formation and atherosclerosis by altering macrophage glycosaminoglycan chain. *Arterioscler Thromb Vasc Biol*. 2021;1076–1091. doi: 10.1161/ATVBAHA.120.315789

20. Anggraeni VY, Emoto N, Yagi K, Mayasari DS, Nakayama K, Izumikawa T, Kitagawa H, Hirata K. Correlation of C4ST-1 and ChGn-2 expression with chondroitin sulfate chain elongation in atherosclerosis. *Biochem Biophys Res Commun*. 2011;406:36–41. doi: 10.1016/j.bbrc.2011.01.096

21. Melgar-Lesmes P, Sánchez-Herrero A, Lozano-Juan F, De La Torre Hernández JM, Montell E, Jiménez W, Edelman ER, Balcells M. Chondroitin sulphate attenuates atherosclerosis in ApoE knockout mice involving cellular regulation of the inflammatory response. *Thromb Haemost*. 2018;118:1329–1339. doi: 10.1055/s-0038-1657753

22. Takeuchi K, Yoshioka N, Higa Onaga S, Watanabe Y, Miyata S, Wada Y, Kudo C, Okada M, Ohko K, Oda K, et al. Chondroitin sulphate N-acetylgalactosaminyl-transferase-1 inhibits recovery from neural injury. *Nat Commun*. 2013;4:1–11. doi: 10.1038/ncomms3740

23. Rockman HA, Ross RS, Harris AN, Knowlton KU, Steinhelper ME, Field LJ, Ross J, Chien KR. Segregation of atrial-specific and inducible expression of an atrial natriuretic factor transgene in an in vivo murine model of cardiac hypertrophy. *Proc Natl Acad Sci*. 1991;88:9907. doi: 10.1073/pnas.88.21.9907a

24. Tournoux F, Petersen B, Thibault H, Zou L, Raher MJ, Kurtz B, Halpern EF, Chaput M, Chao W, Picard MH, et al. Validation of noninvasive measurements of cardiac output in mice using echocardiography. *J Am Soc Echocardiogr*. 2011;24:465–470. doi: 10.1016/j.echo.2010.12.019

25. Gao S, Ho D, Vatner DE, Vatner SF. Echocardiography in mice. *Curr Protoc Mouse Biol*. 2011;1:71–83. doi: 10.1002/9780470942390.mo100130

26. Vinhas M, Araújo AC, Ribeiro S, Rosário LB, Belo JA. Transthoracic echocardiography reference values in juvenile and adult 129/Sv mice. *Cardiovasc Ultrasound*. 2013;11:1–10. doi: 10.1186/1476-7120-11-12

27. Collins KA, Korcarz CE, Shroff SG, Bednarz JE, Fentzke RC, Lin H, Leiden JM, Lang RM. Accuracy of echocardiographic estimates of left ventricular mass in mice. *Am J Physiol - Hear Circ Physiol*. 2001;280:1954–1962. doi: 10.1152/ajpheart.2001.280.5.h1954

28. Teekakirikul P, Eminaga S, Toka O, Alcalai R, Wang L, Wakimoto H, Nayor M, Konno T, Gorham JM, Wolf CM, et al. Cardiac fibrosis in mice with hypertrophic cardiomyopathy is mediated by non-myocyte proliferation and requires Tgf-β. *J Clin Invest*. 2010;120:3520–3529. doi: 10.1172/JCI42028

29. Abràmoff DMD, Magalhães DPJ, Ram DSJ. Image Processing with ImageJ. *Biophotonics Int*. 2004;11:36–42.

30. Mahmood T, Yang PC. Western blot: technique, theory, and troubleshooting. *N Am J Med Sci*. 2012;4:429–434. doi: 10.4103/1947-2714.100998

31. Zafeiriou MP, Noack C, Zelarayan LC. Isolation and primary culture of adult mouse cardiac fibroblasts. *Bio-protocol*. 2016;6:e1860. doi: 10.21769/BioProtoc.1860

32. Ogata T, Ueyama T, Isodono K, Tagawa M, Takehara N, Kawashima T, Harada K, Takahashi T, Matsubara H, et al. MURC, a muscle-restricted coiled-coil protein that modulates the Rho/ROCK pathway, induces cardiac dysfunction and conduction disturbance. *Mol Cell Biol*. 2008;28:3424–3436. doi: 10.1128/mcb.02186-07

33. Rysä J, Tokola H, Ruskoaho H. Mechanical stretch induced transcriptomic profiles in cardiac myocytes. *Sci Rep*. 2018;8:1–14. doi: 10.1038/s41598-018-23042-w

34. Leychenko A, Konorev E, Jijiwa M, Matter ML. Stretch-induced hypertrophy activates NFkB-mediated VEGF secretion in adult cardiomyocytes. *PLoS One*. 2011;6:1–9. doi: 10.1371/journal.pone.0029055

35. Pikkarainen S, Tokola H, Majalahti-Palviainen T, Kerkelä R, Hautala N, Bhalla SS, Charron F, Nemer M, Vuolteenaho O, Ruskoaho H. GATA-4 is a nuclear mediator of mechanical stretch-activated hypertrophic

program. *J Biol Chem*. 2003;278:23807–23816. doi: 10.1074/jbc.M3027 19200

36. Barbosa I, Garcia S, Barbier-Chassefière V, Caruelle JP, Martelly I, Papy-García D. Improved and simple micro assay for sulfated glycosaminoglycans quantification in biological extracts and its use in skin and muscle tissue studies. *Glycobiology*. 2003;13:647–653. doi: 10.1093/glycob/cwg082

37. Huynh MB, Morin C, Carpentier G, Garcia-Filipe S, Talhas-Perret S, Barbier-Chassefière V, Van Kuppevelt TH, Martelly I, Albanese P, Papy-Garcia D. Age-related changes in rat myocardium involve altered capacities of glycosaminoglycans to potentiate growth factor functions and Heparan sulfate-altered Sulfation. *J Biol Chem*. 2012;287:11363–11373. doi: 10.1074/jbc.M111.335901

38. Fan D, Takawale A, Lee J, Kassiri Z. Cardiac fibroblasts, fibrosis and extracellular matrix remodeling in heart disease. *Fibrogenes Tissue Repair*. 2012;5:15. doi: 10.1186/1755-1536-5-15

39. Ivey MJ, Tallquist MD. Defining the cardiac fibroblast. *Circ J*. 2016;80:2269–2276. doi: 10.1253/circj.CJ-16-1003

40. Tallquist MD. Cardiac fibroblasts: from origin to injury. *Curr Opin Physiol*. 2018;1:75–79. doi: 10.1016/j.cophys.2017.08.002

41. Toyama-Sorimachi N, Kitamura F, Habuchi H, Tobita Y, Kimata K, Miyasaka M. Widespread expression of chondroitin sulfate-type serglycins with CD44 binding ability in hematopoietic cells. *J Biol Chem*. 1997;272:26714–26719. doi: 10.1074/jbc.272.42.26714

42. Fujimoto T, Kawashima H, Tanaka T, Hirose M, Toyama-Sorimachi N, Matsuzawa Y, Miyasaka M. CD44 binds a chondroitin sulfate proteoglycan, aggrecan. *Int Immunol*. 2001;13:359–366. doi: 10.1093/intimm/13.3.359

43. Sugahara KN, Hirata T, Tanaka T, Ogino S, Takeda M, Terasawa H, Shimada I, Tamura J-I, ten Dam GB, van Kuppevelt TH, et al. Chondroitin sulfate E fragments enhance CD44 cleavage and CD44-dependent motility in tumor cells. *Cancer Res*. 2008;68:7191–7199. doi: 10.1158/0008-5472.CAN-07-6198

44. Wang J, Zhao W, Chen H, Qin A, Zhu P. Anti-tumor study of chondroitin sulfate-methotrexate Nanogels. *Nanoscale Res Lett*. 2017;12:6–13. doi: 10.1186/s11671-017-2324-1

45. Lin YH, Yang-Yen HF. The osteopontin-CD44 survival signal involves activation of the Phosphatidylinositol 3-Kinase/Akt signaling pathway. *J Biol Chem*. 2001;276:46024–46030. doi: 10.1074/jbc.M105132200

46. Baaten BJG, Li CR, Deiro MF, Lin MM, Linton PJ, Bradley LM. CD44 regulates survival and memory development in Th1 cells. *Immunity*. 2010;32:104–115. doi: 10.1016/j.immuni.2009.10.011

47. Baaten BJG, Li CR, Bradley LM. Multifaceted regulation of T cells by CD44. *Commun Integr Biol*. 2010;3:508–512. doi: 10.4161/cib.3.6.13495

48. Yu S, Cai X, Wu C, Wu L, Wang Y, Liu Y, Yu Z, Qin S, Ma F, Thiery JP, et al. Adhesion glycoprotein CD44 functions as an upstream regulator of a network connecting ERK, AKT and Hippo-YAP pathways in cancer progression. *Oncotarget*. 2015;6:2951–2965. doi: 10.18632/oncotarget.3095

49. Liu S, Cheng C. Akt signaling is sustained by a CD44 splice isoform–mediated positive feedback loop. *Cancer Res*. 2017;77:3791–3801. doi: 10.1158/0008-5472.CAN-16-2545

50. Wang W, Zhang H, Liu S, Kim CK, Xu Y, Hurley LA, Nishikawa R, Nagane M, Hu BO, Stegh AH, et al. Internalized CD44s splice isoform attenuates EGFR degradation by targeting Rab7A. *Proc Natl Acad Sci*. 2017;114:8366–8371. doi: 10.1073/pnas.1701289114

51. Thanee M, Dokduang H, Kittirat Y, Phetcharaburanin J, Klanrit P, Titapun A, Namwat N, Khuntikeo N, Wangwiwatsin A, Saya H, et al. CD44 modulates metabolic pathways and altered ROS-mediated Akt signal promoting cholangiocarcinoma progression. *PLoS One*. 2021;16:1–23. doi: 10.1371/journal.pone.0245871

52. Møller AV, Jørgensen SP, Chen JW, Larnkjær A, Ledet T, Flyvbjerg A, Frystyk J. Glycosaminoglycans increase levels of free and bioactive IGF-I in vitro. *Eur J Endocrinol*. 2006;155:297–305. doi: 10.1530/eje.1.02203

53. Asada M, Shinomiya M, Suzuki M, Honda E, Sugimoto R, Ikekita M, Imamura T. Glycosaminoglycan affinity of the complete fibroblast growth factor family. *Biochim Biophys Acta - Gen Subj*. 2009;1790:40–48. doi: 10.1016/j.bbagen.2008.09.001

54. Mizumoto S, Fongmoon D, Sugahara K. Interaction of chondroitin sulfate and dermatan sulfate from various biological sources with heparin-binding growth factors and cytokines. *Glycoconj J*. 2013;30:619–632. doi: 10.1007/s10719-012-9463-5

55. Sirko S, Von Holst A, Weber A, Wizenmann A, Theocharidis U, Götz M, Faissner A. Chondroitin sulfates are required for fibroblast growth factor-2-dependent proliferation and maintenance in neural stem cells and for epidermal growth factor-dependent migration of their progeny. *Stem Cells*. 2010;28:775–787. doi: 10.1002/stem.309

56. Afratis N, Gialeli C, Nikitovic D, Tsegenidis T, Karousou E, Theocharis AD, Pavão MS, Tzanakakis GN, Karamanos NK. Glycosaminoglycans: key players in cancer cell biology and treatment. *FEBS J*. 2012;279:1177–1197. doi: 10.1111/j.1742-4658.2012.08529.x

57. Nikitovic D, Assouti M, Sifaki M, Katonis P, Krasagakis K, Karamanos NK, Tzanakakis GN. Chondroitin sulfate and heparan sulfate-containing proteoglycans are both partners and targets of basic fibroblast growth factor-mediated proliferation in human metastatic melanoma cell lines. *Int J Biochem Cell Biol*. 2008;40:72–83. doi: 10.1016/j.biocel.2007.06.019

58. Fthenou E, Zafiropoulos A, Tsatsakis A, Stathopoulos A, Karamanos NK, Tzanakakis GN. Chondroitin sulfate A chains enhance platelet derived growth factor-mediated signalling in fibrosarcoma cells. *Int J Biochem Cell Biol*. 2006;38:2141–2150. doi: 10.1016/j.biocel.2006.06.006

59. Asimakopoulou AP, Theocharis AD, Tzanakakis GN, Karamanos NK. The biological role of chondroitin sulfate in cancer and chondroitin-based anticancer agents. *In Vivo*. 2008;22:385–389.

60. Sirko S, Von Holst A, Wizenmann A, Götz M, Faissner A. Chondroitin sulfate glycosaminoglycans control proliferation, radial glia cell differentiation and neurogenesis in neural stem/progenitor cells. *Development*. 2007;134:2727–2738. doi: 10.1242/dev.02871

61. Igarashi N, Takeguchi A, Sakai S, Akiyama H, Higashi K, Toida T. Effect of molecular sizes of chondroitin sulfate on interaction with L-selectin. *Int J Carbohydr Chem*. 2013;2013:1–9. doi: 10.1155/2013/856142

62. Lim JJ, Temenoff JS. The effect of desulfation of chondroitin sulfate on interactions with positively charged growth factors and upregulation of cartilaginous markers in encapsulated MSCs. *Biomaterials*. 2013;34:5007–5018. doi: 10.1016/j.biomaterials.2013.03.037

63. Karumbaiah L, Enam SF, Brown AC, Saxena T, Betancur MI, Barker TH, Bellamkonda RV. Chondroitin sulfate glycosaminoglycan hydrogels create endogenous niches for neural stem cells. *Bioconjug Chem*. 2015;26:2336–2349. doi: 10.1021/acs.bioconjchem.5b00397

64. Djerbal L, Lortat-Jacob H, Kwok J. Chondroitin sulfates and their binding molecules in the central nervous system. *Glycoconj J*. 2017;34:363–376. doi: 10.1007/s10719-017-9761-z

65. Garcia-Menendez L, Karamanlidis G, Kolwicz S, Tian R. Substrain specific response to cardiac pressure overload in C57BL/6 mice. *Am J Physiol - Hear Circ Physiol*. 2013;305(3):H397–H402. doi: 10.1152/ajpheart.00088.2013

66. Finsen AV, Lunde IG, Sjaastad I, Østli EK, Lyngra M, Jarstadmarken HO, Hasic A, Nygård S, Wilcox-Adelman SA, Goetinck PF, et al. Syndecan-4 is essential for development of concentric myocardial hypertrophy via stretch-induced activation of the calcineurin-NFAT pathway. *PLoS One*. 2011;6(12):e28302. doi: 10.1371/journal.pone.0028302

67. Martin TP, Robinson E, Harvey AP, Macdonald M, Grieve DJ, Paul A, Currie S. Surgical optimization and characterization of a minimally invasive aortic banding procedure to induce cardiac hypertrophy in mice. *Exp Physiol*. 2012;97:822–832. doi: 10.1113/expphysiol.2012.065573

68. Creemers EE, Pinto YM. Molecular mechanisms that control interstitial fibrosis in the pressure-overloaded heart. *Cardiovasc Res*. 2011;89:265–272. doi: 10.1093/cvr/cvq308

69. Dai Z, Aoki T, Fukumoto Y, Shimokawa H. Coronary perivascular fibrosis is associated with impairment of coronary blood flow in patients with non-ischemic heart failure. *J Cardiol*. 2012;60:416–421. doi: 10.1016/j.jjcc.2012.06.009

70. LaFramboise WA, Scalise D, Stoodley P, Graner SR, Guthrie RD, Magovern JA, Becich MJ. Cardiac fibroblasts influence cardiomyocyte phenotype in vitro. *Am J Physiol - Cell Physiol*. 2007;292:1799–1808. doi: 10.1152/ajpcell.00166.2006

71. Hall C, Gehmlich K, Denning C, Pavlovic D. Complex relationship between cardiac fibroblasts and cardiomyocytes in health and disease. *J Am Heart Assoc*. 2021;10:1–15. doi: 10.1161/JAHA.120.019338

72. Xiang F-L, Fang M, Yutzey KE. Loss of β-catenin in resident cardiac fibroblasts attenuates fibrosis induced by pressure overload in mice. *Nat Commun*. 2017;8:712. doi: 10.1038/s41467-017-00840-w

73. Pedrotty DM, Klinger RY, Kirkton RD, Bursac N. Cardiac fibroblast paracrine factors alter impulse conduction and ion channel expression of neonatal rat cardiomyocytes. *Cardiovasc Res*. 2009;83:688–697. doi: 10.1093/cvr/cvp164

74. Zhang XI, Shen MR, Xu ZD, Hu Z, Chen C, Chi YL, Kong ZD, Li ZF, Li XT, Guo SL, et al. Cardiomyocyte differentiation induced in cardiac progenitor cells by cardiac fibroblast-conditioned medium. *Exp Biol Med*. 2014;239:628–637. doi: 10.1177/1535370214525323

75. Carver W, Nagpal ML, Nachtigal M, Borg TK, Terracio L. Collagen expression in mechanically stimulated cardiac fibroblasts. *Circ Res*. 1991;69:116–122. doi: 10.1161/01.RES.69.1.116

76. Lee AA, Delhaas T, McCulloch AD, Villarreal FJ. Differential responses of adult cardiac fibroblasts to in vitro biaxial strain patterns. *J Mol Cell Cardiol*. 1999;31:1833–1843. doi: 10.1006/jmcc.1999.1017

77. Prante C, Milting H, Kassner A, Farr M, Ambrosius M, Schön S, Seidler DG, Banayosy AE, Körfer R, Kuhn J, et al. Transforming growth factor β1-regulated xylosyltransferase I activity in human cardiac fibroblasts and its impact for myocardial remodeling. *J Biol Chem*. 2007;282:26441–26449. doi: 10.1074/jbc.M702299200

78. Bishop JE, Rhodes S, Laurent GJ, Low RB, Stirewalt WS. Increased collagen synthesis and decreased collagen degradation in right ventricular hypertrophy induced by pressure overload. *Cardiovasc Res*. 1994;28:1581–1585. doi: 10.1093/cvr/28.10.1581

79. Ranjan P, Kumari R, Verma SK. Cardiac fibroblasts and cardiac fibrosis: precise role of exosomes. *Front Cell Dev Biol*. 2019;7:1–12. doi: 10.3389/fcell.2019.00318

80. Wu YJ, La Pierre DP, Wu J, Yee AJ, Yang BB. The interaction of versican with its binding partners. *Cell Res*. 2005;15:483–494. doi: 10.1038/sj.cr.7290318

81. Shipp EL, Hsieh-Wilson LC. Profiling the sulfation specificities of glycosaminoglycan interactions with growth factors and chemotactic proteins using microarrays. *Chem Biol*. 2007;14:195–208. doi: 10.1016/j.chembiol.2006.12.009

82. Zhang F, Zheng L, Cheng S, Peng Y, Fu L, Zhang X, Linhardt RJ. Comparison of the interactions of different growth factors and glycosaminoglycans. *Molecules*. 2019;24:1–13. doi: 10.3390/molecules24183360

83. ten Dam GB, van de Westerlo EMA, Purushothaman A, Stan RV, Bulten J, Sweep FCGJ, Massuger LF, Sugahara K, van Kuppevelt TH. Antibody GD3G7 selected against embryonic glycosaminoglycans defines chondroitin sulfate-E domains highly up-regulated in ovarian cancer and involved in vascular endothelial growth factor binding. *Am J Pathol*. 2007;171:1324–1333. doi: 10.2353/ajpath.2007.070111

SUPPLEMENTAL MATERIAL

Table S1. Major Resources.

Antibodies

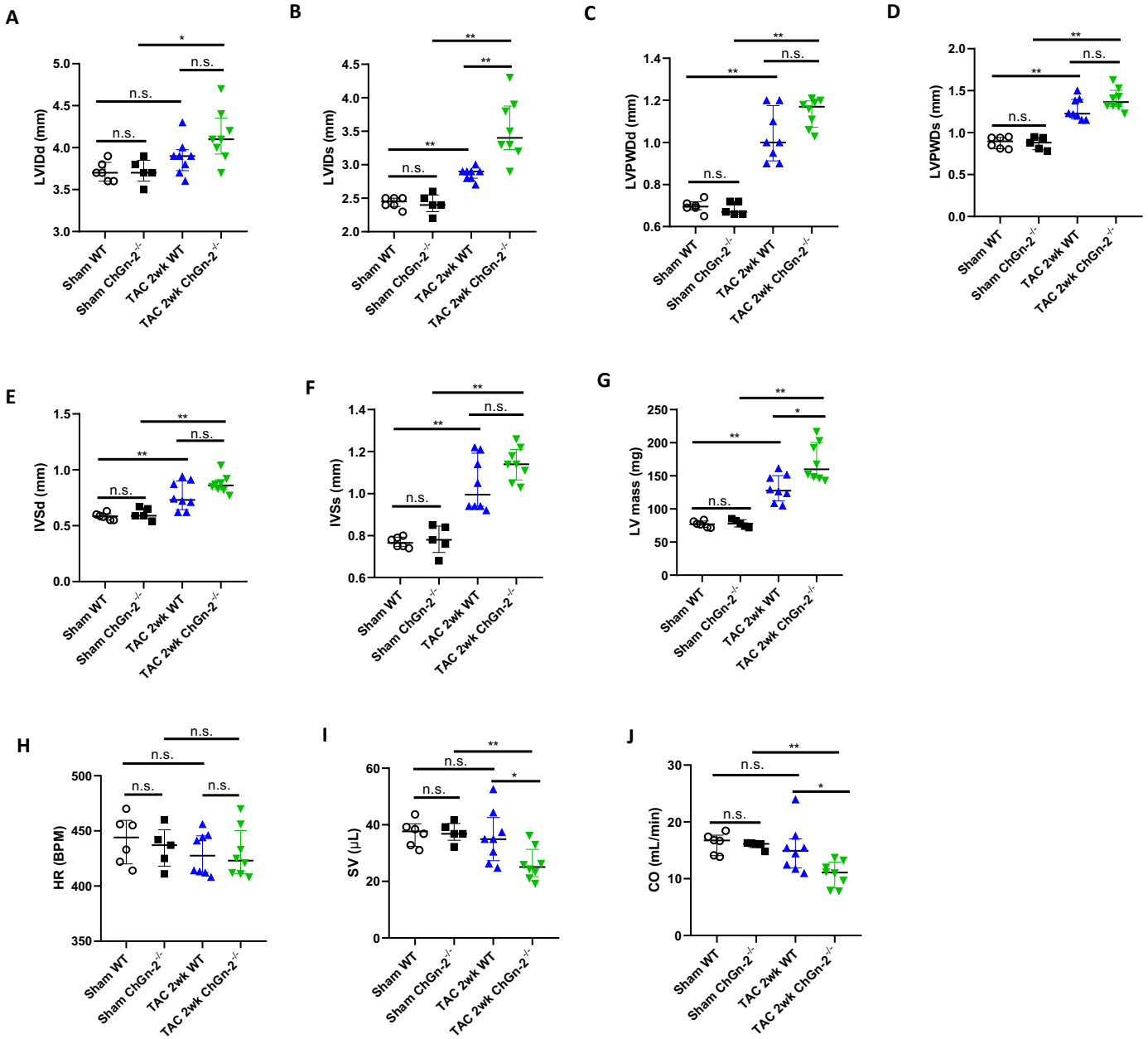| Target antigen	Vendor or Source	Catalog #	Working concentration
Rabbit polyclonal anti-CSGalNact-2	Protein tech	17420-1-AP	1 : 1000 dilution (WB)
Goat anti mouse decorin	R&D System	AF1060-SP	1 : 1000 dilution (WB)
GAPDH (14C10) Rabbit mAB	Cell Signaling Technology	2118S	1 : 2000 dilution (WB)
Cleaved Caspase-3 (Asp175) Antibody Rabbit mAB	Cell Signaling Technology	9661S	1 : 2000 dilution (WB)
Caspase-3 Antibody Rabbit mAB	Cell Signaling Technology	9662S	1 : 2000 dilution (WB)
Phospho-Akt (Ser473) Antibody Rabbit mAB	Cell Signaling Technology	9271S	1 : 1000 dilution (WB)
Akt Antibody Rabbit mAB	Cell Signaling Technology	9272S	1 : 2000 dilution (WB)
Purified Rat Anti CD44 (IM7 clone)	BD Pharmingen™	553131	1: 1000 dilution (WB) 1: 200 dilution (in vitro cell treatment)
Anti Chondroitin Sulfate A (2H6)	Cosmo Bio	NU-07-001	1 : 5000 dilution (dot blot) 1 : 200 dilution (IF)
Anti-rabbit IgG, HRP-linked Antibody	Cell Signaling Technology	7074	1: 3000 dilution (WB)
Anti-rat IgG, HRP-linked Antibody	Cell Signaling Technology	7077	1: 3000 dilution (WB)
Peroxidase-AffiniPure Donkey Anti-Goat IgG (H+L)	Jackson Immunoresearch	705-035-147	1 : 3000 dilution (WB)
Goat anti-mouse IgM FITC conjugate	TCI Chemicals	G0453	1:200 dilution (IF)
Goat anti-mouse IgM HRP conjugate	TCI Chemicals	G0417	1: 2000 dilution (dot blot)
Anti-Cardiac troponin T	Abcam	Ab10214	1 : 400 dilution (IF)
Donkey anti-mouse IgG alexa fluor 594	Invitrogen	A-21203	1 : 500 dilution (IF)

Reagents

Name	Vendor or Source	Catalog #
1,9-dimethylmethylene (DMMB)	Sigma-aldrich	341088
2-Amino-2-hydroxymethyl-1,3-propanediol (Tris(hydroxymethyl)aminomethane)	Wako pure chemicals	207-06275
4% Paraformaldehyde phosphate buffer Solution	Wako pure chemicals	163-20145
ABAM	Gibco	15240062
Acetic acid	Wako pure chemicals	017-00256
Alcian blue staining pH 1.0 (for tissue)	Muto pure chemicals	40862
Can Get Signal®	Toyobo	NKB-101
Chondroitin sulfate A sodium salt from bovine trachea	Sigma-aldrich	39455-18-0
Chondroitinase ABC	Sigma-aldrich	C3667
Clarity Western ECL Substrate	Bio-Rad	1705061
DC™ protein assay	Bio-rad	5000116EN
DISMIC-13CP syringe filter	Advantec	13CP020AS
Dulbecco's Modified Eagle's Medium – high glucose	Sigma-aldrich	D5796
Ethanol	Wako pure chemicals	057-00456
Fetal bovine serum (FBS)	Gibco	10270106
Fibroblast Growth Medium	PromoCell	C-23110
Glycine	Sigma-aldrich	12-1210-5
in situ Cell Death Detection Kit	Roche	11684795910
LightCycler® FastStart DNA Master SYBR Green I	Roche	03003230001
M.O.M immunodetection kit	Vector Laboratories	PK-2200
Mayer's hematoxylin	Muto pure chemicals	3000-2
Nucleo Spin RNA Clean Up kit	Macherey-Nagel	740948.50
pcDNA™3.1/Myc-His vector	Invitrogen	V80020
Penicillin-streptomycin (P/S)	Thermo fisher	15140122
PrimeScript™ RT reagent Kit with gDNA Eraser	TaKaRa	RR 047 A
Protease Inhibitor Coctail	Sigma-aldrich	P8340
Sodium chloride (NaCl)	Wako pure chemicals	191-01665
Sodium Orthovanadate	Wako pure chemicals	198-09752
Sodium Fluoride	Wako pure chemicals	192-01972
Vectashield mounting with DAPI	Vector labs	H-1200

Table S2. List of primers used in real time PCR.

Gene	Primer sequence
Human ChGn-2	F = 5'-CTGACCATTGGTGGATTTGACAT-3'
	R = 5'-AACCGGAGTCCGAATCACAA-3'
Human IGF-1	F = 5'-CCGGAGCTGTGATCTAAGGA-3'
	R = 5'-CCTGCACTCCCTCTACTTGC-3'
Human bFGF	F =5 '-AGAGCGACCCTCACATCAAG-3'
	R = 5'-ACTGCCCAGTTCGTTTCAGT-3'
Human PDGFa	F = 5'-CAAGACCAGGACGGTCATTT-3'
	R = 5'-CCTGACGTATTCCACCTTGG-3'
Human GCSF	F = 5'-GCTTGAGCCAACTCCATAGC-3'
	R = 5'-TTCCCAGTTCTTCCATCTGC-3'
Rat ANP	F = 5'-CTTCCTCTTCCTGGCCTTTTG-3'
	R = 5'-TGTGTTGGACACCGCACTGTA-3'
Rat BNP	F = 5'-AGCTGCTTTGGGCAGAAGAT-3'
	R = 5'-AAAACAACCTCAGCCCGTCA-3'
Rat GAPDH	F = 5'-GGCACAGTCAAGGCTGAGAATG-3'
	R = 5'-TCTCGCTCCTGGAAGATGGTGA-3'
Human and mouse 18S rRNA	F = 5'-GTAACCCGTTGAACCCCATT-3'
	R = 5'-CCATCCAATCGGTAGTAGCG-3'
Mouse ChGn-2	F = 5'-AGAGGCAGGTGGATTTCTGA-3'
	R = 5'-ACAACAAAGAGCTCCCCAAC-3'
Mouse Col1a1	F = 5'-ATGCCGCGACCTCAAGATG-3'
	R = 5'-TGAGGCACAGACGGCTGAGTA-3'

Figure S1. Echocardiographic measurements for male WT and ChGn-2$^{-/-}$ mice.

(A) Echocardiographic measurement of LVIDd in either sham or TAC group 2 weeks after surgery.

(B) Echocardiographic measurement of LVIDs in either sham or TAC group 2 weeks after surgery.

(C) Echocardiographic measurement of LVPWDd in either sham or TAC group 2 weeks after surgery.

(D) Echocardiographic measurement of LVPWDs in either sham or TAC group 2 weeks after surgery.

(E) Echocardiographic measurement of IVSd in either sham or TAC group 2 weeks after surgery.

(F) Echocardiographic measurement of IVSs in either sham or TAC group 2 weeks after surgery.

(G) Echocardiographic measurement of LV mass in either sham or TAC group 2 weeks after surgery.

(H) Echocardiographic measurement of HR in either sham or TAC group 2 weeks after surgery.

(I) Echocardiographic measurement of SV in either sham or TAC group 2 weeks after surgery.

(J) Echocardiographic measurement of CO in either sham or TAC group 2 weeks after surgery.

Abbreviation used are ; LVID = Left ventricle internal diameter; LVPWD = Left ventricle posterior wall diameter; IVS = Interventricular septum; LV mass = Left ventricular mass; HR = Heart rate; SV = Stroke volume; CO = Cardiac output; -d = in diastole; -s = in systole.

Data represent median and interquartile range. *P < 0.05, **P < 0.01, and ***P < 0.001. n.s., not significant. Statistical analyses were performed using Kruskal-Wallis test followed by Willcoxon rank-sum test (A-J).

**Figure S2. Survival rate after TAC surgery in male WT and ChGn-2-/- mice.**
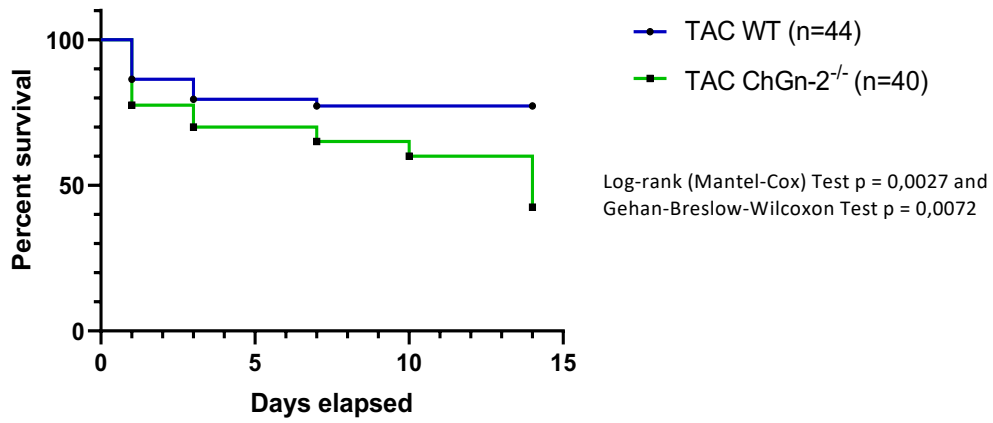
Kaplan-Meier estimate curve for survival after TAC surgery in WT and ChGn-2-/- mice during the experimental period. Statistical analyses for differences between WT and ChGn-2-/- mice were performed using Log-rank (Mantel-Cox) test (p = 0.0027) and Gehan-Breslow-Wilcoxon test (p = 0.0072).
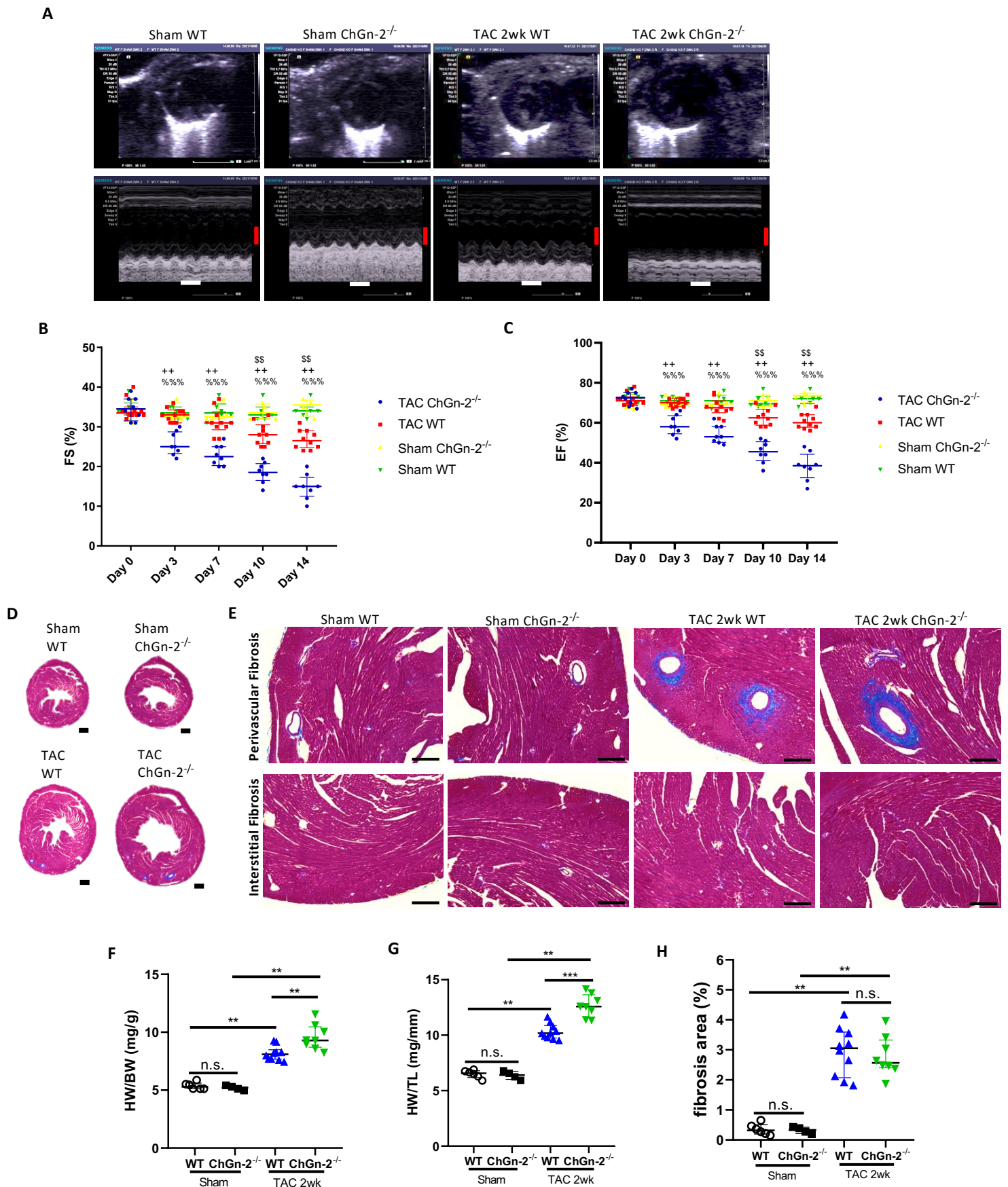
Figure S3. Cardiac functions and morphologies in female WT and ChGn-2$^{-/-}$ mice after TAC.
(A) Representative echocardiographic images in female WT and ChGn-2-/- mice in either sham or TAC group 2 weeks after surgery. White bars: 200 msec. Red bars: 2 mm. (B, C) Left ventricular systolic function was analyzed by the fractional shortening (FS) (B) and ejection fraction (EF) (C) at day 0, 3, 7, 10, and 14 days after TAC (n = 5 for sham WT, n = 4 for sham ChGn-2$^{-/-}$, n = 10 for TAC WT, n = 8 for TAC ChGn-2$^{-/-}$). Kruskal-Wallis test followed by Willcoxon rank-sum test was used to compare the FS and EF of each group at each time point. $P < 0.05, $$P < 0.01, and $$$P < 0.001 between sham WT and TAC WT. +P < 0.05, ++P < 0.01, and +++P < 0.001 between sham ChGn-2$^{-/-}$ and TAC ChGn-2$^{-/-}$. %P < 0.05, %%P < 0.01, and %%%P < 0.001 between TAC WT and TAC ChGn-2$^{-/-}$. (D) Representative images for transversal section of the heart of female WT and ChGn-2$^{-/-}$ mice in either sham or TAC group. Bars: 500 μm. (E) Representative images for Masson's trichome staining of the heart in female WT and ChGn-2$^{-/-}$ mice in either sham or TAC group 2 weeks after surgery. Bars: 200 μm. (F, G) Quantification of heart weight (HW) normalized to body weight (BW) (F) or tibia length (TL) (G) in female WT and ChGn-2$^{-/-}$ mice in either sham or TAC group (n = 5 for sham WT, n = 4 for sham ChGn-2$^{-/-}$, n = 10 for TAC WT, n = 8 for TAC ChGn-2$^{-/-}$). (H) Quantification of collagen fibrosis area (%) in the heart of female WT and ChGn-2$^{-/-}$ mice in either sham or TAC group (n = 5 for sham WT, n = 4 for sham ChGn-2$^{-/-}$, n = 10 for TAC WT, n = 8 for TAC ChGn-2$^{-/-}$). Data represent median and interquartile range. *P < 0.05, **P < 0.01, and ***P < 0.001. Statistical analyses were performed using Kruskal-Wallis test followed by Willcoxon rank-sum test (F, G, and H).
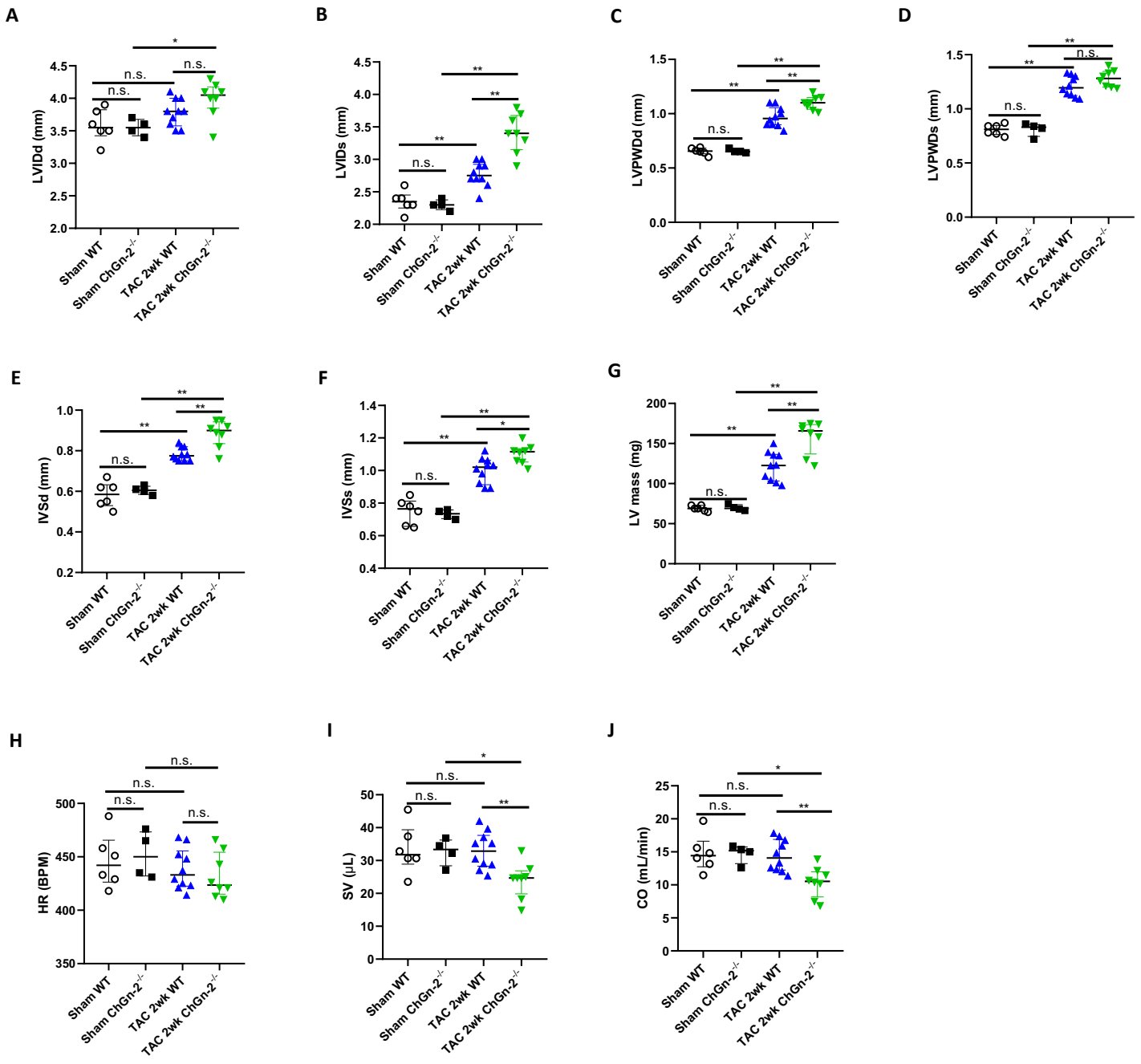
Figure S4. Echocardiographic measurements for female WT and ChGn-2^{-/-} mice.
(A) Echocardiographic measurement of LVIDd in either sham or TAC group 2 weeks after surgery.
(B) Echocardiographic measurement of LVIDs in either sham or TAC group 2 weeks after surgery.
(C) Echocardiographic measurement of LVPWDd in either sham or TAC group 2 weeks after surgery.
(D) Echocardiographic measurement of LVPWDs in either sham or TAC group 2 weeks after surgery.
(E) Echocardiographic measurement of IVSd in either sham or TAC group 2 weeks after surgery.
(F) Echocardiographic measurement of IVSs in either sham or TAC group 2 weeks after surgery.
(G) Echocardiographic measurement of LV mass in either sham or TAC group 2 weeks after surgery.
(H) Echocardiographic measurement of HR in either sham or TAC group 2 weeks after surgery.
(I) Echocardiographic measurement of SV in either sham or TAC group 2 weeks after surgery.
(J) Echocardiographic measurement of CO in either sham or TAC group 2 weeks after surgery.
Abbreviation used are ; LVID = Left ventricle internal diameter; LVPWD = Left ventricle posterior wall diameter; IVS = Interventricular septum; LV mass = Left ventricular mass; HR = Heart rate; SV = Stroke volume; CO = Cardiac output; -d = in diastole; -s = in systole. Data represent median and interquartile range. *P < 0.05, **P < 0.01, and ***P < 0.001. n.s., not significant. Statistical analyses were performed using Kruskal-Wallis test followed by Willcoxon rank-sum test (A-J).

Figure S5. Cardiomyocyte apoptosis assessed by TUNEL and cTnT immunofluorescence staining.
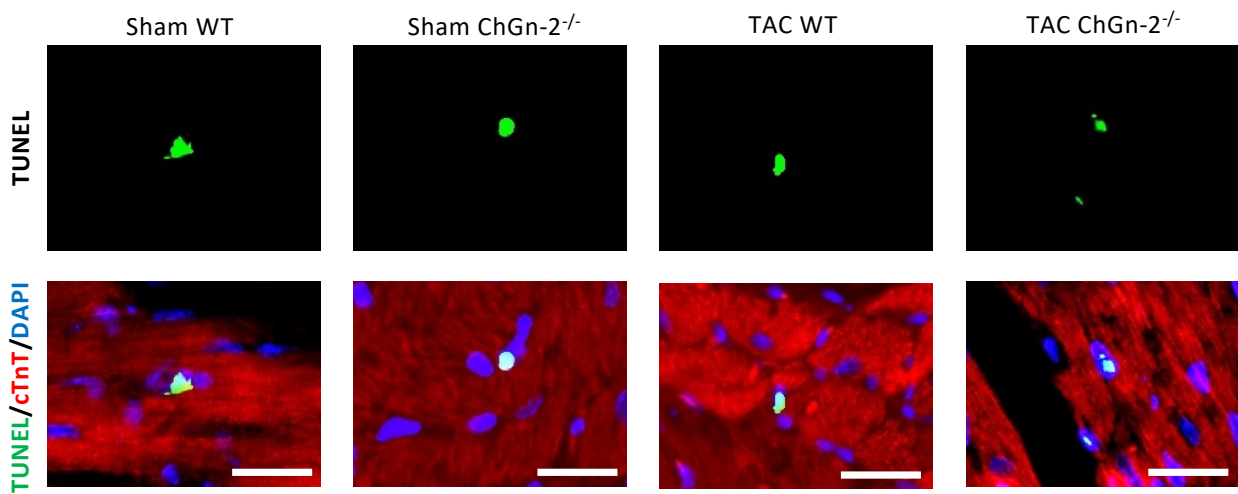

Representative images at high magnification for TUNEL and cardiac troponin T (cTnT) immunofluorescence staining in the heart of WT and ChGn-2$^{-/-}$ mice in either sham or TAC group 2 weeks after surgery. Bars: 25 μm. TUNEL (green), cTnT (red) and DAPI (blue).

Figure S6. Combination treatment with anti-CD44 antibody and LY294002 in H9C2 cells incubated with CS-A.
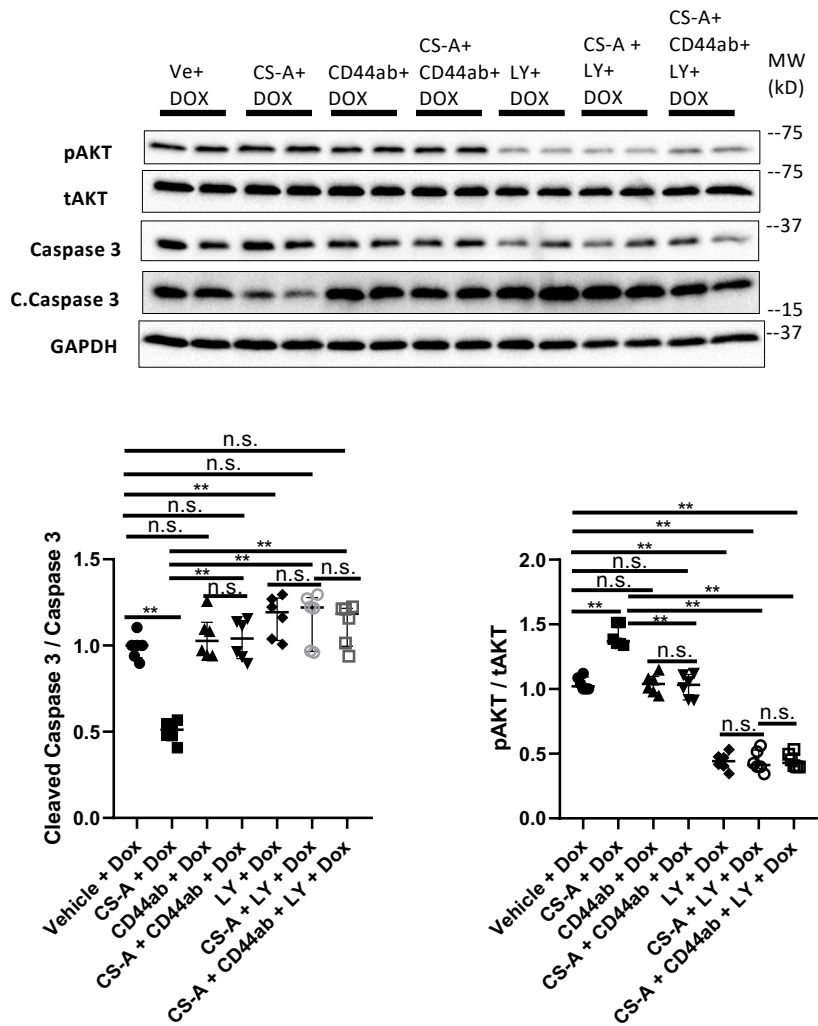
Immunoblotting for caspase-3, cleaved caspase-3, p-Akt, t-Akt, and GAPDH in H9C2 cells treated with either vehicle or CS-A in the presence of DOX. Some cells were treated with PI3K inhibitor, LY294002 (LY), anti-CD44 antibody, or both. CS-A at 500 μg/mL; LY294002 at 25μM; CD44ab at 1: 200 dilutions; DOX at 1 μM were used. Data represent median and interquartile range. *P < 0.05, **P < 0.01, and ***P < 0.001. n.s., not significant. Statistical analyses were performed using Kruskal-Wallis test followed by Willcoxon rank-sum test.

Figure S7. IGF-1 concentration in CM derived from HCFs.
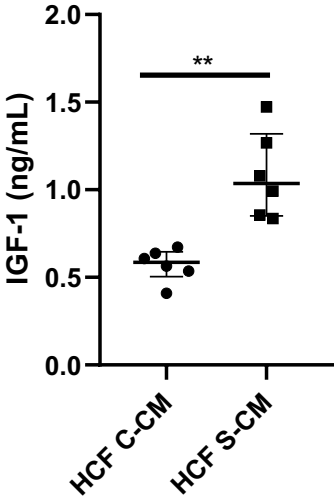
IGF-1 concentration was analyzed using enzyme-linked immunosorbent assay (ELISA) in CMs derived from HCFs in either control (C-CM) or stretch (S-CM) condition (n = 6 for each group). Data represent median and interquartile range. **P < 0.01. Statistical analyses were performed using Willcoxon rank-sum test.

**Figure S8. Scheme for CS-A and IGF-1 binding experiments.**

Coating with PBS or CS-A 200 μg/mL or CS-A 200 μg/mL + ChABC 10 mIU/mL at 37°C for 24h. Two sets of plates were prepared

PBS **CS-A** **CS-A + ChABC**

Wash PBS 2x

Incubation with IGF-1 100 ng/mL or PBS at 37°C for 2h, followed by washing with PBS

PBS **IGF-1** **PBS** **IGF-1** **PBS** **IGF-1**

Wash PBS 2x

Cells were plated in serum free DMEM free, and incubate at 37°C for 24h. RNAs were collected at this point in one set of the plates (for Fig 7B). Cells in another set proceed to next step.

As a positive control IGF-1 100 ng/mL were added in the medium at the time of cell plating

Subsequently, 1 μM DOX was added into the medium, and cells were incubated in the medium at 37°C for 3h. Finally, proteins were collected from cells (for Fig 7C).

Protein isolation and western blotting

RNA isolation and quantitative RT-PCR
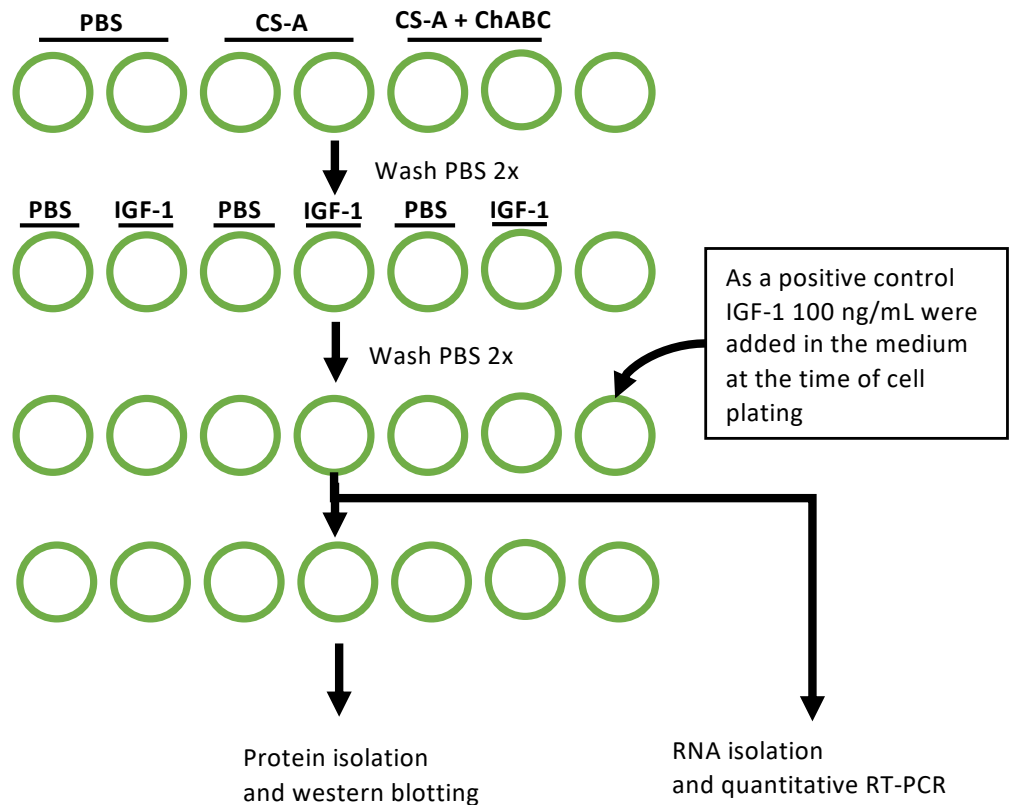
Culture plates were coated with CS-A in the presence or absence of ChABC for 24h at 37°C. Negative control plates were prepared by incubating with PBS. Two sets of plates were prepared. After washing with PBS, plates were incubated with IGF-1 or PBS for 2 h at 37°C, followed by 2 times of washing with PBS. H9C2 cells were then seeded onto the plates and incubated in the serum free DMEM medium for 24 h. Then, RNAs were isolated from one set of plates. Cells in another set of plate were treated with DOX for 3 h before lysed for protein extraction.

Figure S9. Schematic diagram of dual pathway for cardioprotective effects mediated by CS-GAGs chain.